Renewable and Sustainable Energy Reviews 37 (2014) 100–122

Contents lists available at ScienceDirect

Renewable and Sustainable Energy Reviews

journal homepage: www.elsevier.com/locate/rser

A review of thermohydraulic performance of artificially roughened solar air heaters

Anil Kumar [a,*], R.P. Saini [b], J.S. Saini [c]

[a] Mechanical Engineering Department, Shoolini University, Solan, Himachal Pradesh 174212, India
[b] Alternate Hydro Energy Centre, Indian Institute of Technology Roorkee, Roorkee, Uttarakhand 247667, India
[c] Mechanical & Industrial Engineering Department, Indian Institute of Technology Roorkee, Roorkee, Uttarakhand 247667, India

ARTICLE INFO

Article history:
Received 9 October 2012
Received in revised form
3 April 2014
Accepted 27 April 2014
Available online 27 May 2014

Keywords:
Solar air heater
Exergetic efficiency
Thermohydraulic performance

ABSTRACT

Solar air heaters form the major component of solar energy utilization system which absorbs the incoming solar radiation, converting it into thermal energy at the absorbing surface, and transferring the energy to a fluid flowing through the collector. The efficiency of flat plate solar air heater has been found to be low because of low convective heat transfer coefficient between absorber plate and the flowing air which increases the absorber plate temperature, leading to higher heat losses to the environment resulting in low thermal efficiency of such collectors. Artificial roughness in the form of repeated ribs is the most effective and economic way of improving the thermal performance of solar air heater. This paper presents an extensive review on the research carried out on artificial roughened solar air heater ducts. The objective of this paper is to review various studies, carried out on thermal as well as hydraulic performance of artificial roughened solar air heater ducts. The review presented in this paper will be useful for the researchers working in this area.

Contents

1. Introduction

Energy is a basic ingredient needed to sustain life and development. Energy is needed in various forms to fulfil our day to day requirements. Energy consumption rates of the people are directly

* Corresponding author. Tel.: +91 8627966839.
E-mail address: anil_aheciit@yahoo.com (A. Kumar).

http://dx.doi.org/10.1016/j.rser.2014.04.063
1364-0321/

Nomenclature

A_p	Area of heated plate, m^2
C_p	Specific heat of fluid at constant pressure, J/(kg K)
G	Mass velocity of fluid through the collector, kg/(m^2 s)
G_d	Gap or discrete distance, m
G_p	Gap or discrete position, m
G_r	Grashof number
G_P/Lv	Relative discrete or gap position
D	Hydraulic diameter of duct, m
e	Rib height, m
e/D	Relative roughness height
f_s	Friction factor of smooth duct
f	Friction factor of roughened duct
F'	Plate efficiency number
F_o	Heat removal factor
g	Gap or discrete width, m
g/e	Relative gap or discrete width
H	Depth of duct, m
h	Convective heat transfer coefficient, W/(m^2 K)
I	Solar intensity, W/m^2
k	Thermal conductivity of air, W/(m K)
L	Length of test section, m
L_v	Length of single v-rib, m
m	Mass flow rate, kg/s
Nu	Nusselt number of roughened duct
Nu_s	Nusselt number of smooth duct
P	Pitch of the rib, m
P/e	Relative roughness pitch
Pr	Prandtl number
Q_u	Useful heat gain rate, W
Re	Reynolds number
Ra	Rayleigh number
T_f	Average temperature of air, K
T_s	Temperature of the sun, K
T_i	Initial temperature of air, K
T_o	Final temperature of air, K
T_p	Average plate temperature, K
Ub	Bottom loss coefficient, W/(m^2 K)
Ue	Edge loss coefficient, W/(m^2 K)
U_L	Overall heat loss coefficient, W/(m^2 K)
Ut	Top loss coefficient, W/(m^2 K)
V	Velocity of air, m/s
W	Width of duct, m
w	Width of V-rib, m
W/w	Roughness width ratio
ΔT	Temperature difference
$\Delta T/I$	Performance parameter, K m^2/W

Greek letter symbols

α	Angle of attack, degrees
β'	Collector tilt angle, degrees
η	Thermo-hydraulic performance parameter
ρ	Density of air, kg/m^3
ρ_m	Density of manometric fluid, kg/m^3
μ	Dynamic viscosity of air, N s/m^2
$\tau\alpha$	Absorbance–transmittance product
η_{th}	Thermal efficiency
η_{eff}	Effective efficiency

related to the prosperity or the standard of living. Two types of energy resources are available: conventional and non-conventional [1,2]. Conventional energy resources such as fossil fuels (coal, crude oil and natural gas) are limited in amount. Total energy in recoverable conventional energy resources is estimated to be around 30–35 Q ($1Q=10^{18}$ kJ) while the global energy consumption rate is roughly 0.4–0.5 Q/yr. Hence conventional energy resources are roughly estimated to last for 75–85 years. This awareness of the limited nature of conventional energy resources gave rise to the search of alternate energy resources. Non-conventional or alternate energy resources can be divided into two groups, namely, renewable and non-renewable resources. Renewable resources are those which have a short period of renewal (upto a few years) such as solar energy, wind energy, biomass energy, hydroenergy, ocean and tidal energy. Solar energy is the most promising of all these alternatives [3,4]. Solar energy has the greatest potential among all the sources of renewable energy and even a small amount of this renewable source of energy is sufficient to meet the total energy demand of the world. If we can use 5% of this energy, it will be 50 times what the world will require. Solar energy is readily available, well distributed and inexhaustible for all practical purposes, and has no polluting effects upon the environment when converted and utilized. Solar air heaters, because of their inherent simplicity are cheap and most widely used collector devices. Solar air heaters are being used for many applications for low and moderate temperatures. Some of these are space heating, crop drying, drying of concrete and solar dryer [1,2,5,6,7].

The use of artificial roughness on the underside of the heated plate can substantially enhance the thermal performance of the solar air heater due to increase in convective heat transfer coefficient from the plate to air. Surface roughness is one of the first techniques to be considered as a means of augmenting forced convection heat transfer. In order to attain higher convective heat transfer coefficient it is desirable that the flow at the heat transfer surface should be turbulent. However, the turbulence created in the core can increase the fan power exorbitantly. It is therefore, desirable that the turbulence must be created only very close to the heat transfer surface, i.e. in the laminar sub-layer only, where the heat exchange takes place. However, as pointed out above, it is necessary that while creating turbulence to break the laminar sub-layer, the core flow should not be disturbed so as to avoid excessive losses. This can be achieved by using artificial roughness with roughness height being such that it does not project into the core but is of the height that just project out of laminar sublayer. Numbers of experimental investigations involving roughness elements of different shapes, sizes and orientations with respect to flow direction have been carried out in order to obtain an optimum arrangement of roughness geometry. Hans et al., [8] carried out a review of roughness geometry in solar air heater ducts. They discussed different roughness geometries used in solar air heater ducts and explained the concept of artificial roughness, effects of various roughness parameters on the flow pattern and also briefly discussed and reviewed the roughness geometries used in solar air heater ducts. The objective of this paper is to review various studies, in which different artificial roughness elements are used to enhance the heat transfer rate with little penalty of increase in friction losses and also discuss the thermo-hydraulic (thermal as well as hydraulic) performance of artificial roughened solar air heater ducts.

Table 1
Artificial roughness geometries and parameters investigated by various investigators.

Sr. no.	Investigators	Rib geometry	Parameters
1.	Prasad and Saini [10]	Transverse continuous rib	P/e, e/D
2.	Sahu and Bhagoria [14]	Transverse broken rib	P/e, e/D, α
3.	Gupta et al.[15]	Inclined continuous rib	P/e, e/D, α
4.	Aharwal et al.[16]	Inclined rib with gap	P/e, e/D, α, d/W, g/e
5.	Momin et al.[17]	V-shaped rib	P/e, e/D, α
6.	Singh et al.[37]	Discrete v-rib	d/W, g/e, P/e, e/D, α
7.	Karwa et al.[20]	Chamfered rib	P/e, e/D, ϕ
8.	Saini and Saini [21]	Expanded metal mesh	e/D, S/e, L/e, α
9.	Saini and Saini [22]	Arc shaped rib	e/D, α
10.	Karmare and Tikekar [23]	Metal grit rib	P/e, e/D, l/s
11.	Bhagoria et al. [24]	Wedge shaped rib	P/e, e/D, ϕ
12.	Saini and Verma [25]	Dimpled shaped rib	P/e, e/D
13.	Lanjeware et al. [26]	W-shaped rib	P/e, e/D, α
14.	Kumar and Bhagoria [27]	Discrete w-shaped rib	P/e, e/D, α
15.	Varun et al. [28]	Combination of inclined and transverse rib	P/e, e/D
16.	Jaurker et al. [30]	Rib-groove	P/e, e/D, g/p
17.	Bopche and Tandale [31]	U-shaped rib	P/e, e/D, α
18.	Hans et al. [32]	Multi v-shaped rib	P/e, e/D, α, W/w
19.	Patil et al. [56–58]	Discrete v-rib with combined staggered rib pieces	P'/P, S'/S, r/e, e/D. P/e, α
20.	Sethi et al. [59]	Dimpled shaped rib	P/e, e/D, α
21.	Kumar et al. [60,61]	Multi v-shaped rib with gap	G_d/Lv, g/e, W/w, e/D, P/e, α

2. Artificially roughened solar air heater ducts

The application of artificial roughness in the form of fine wires or ribs having different geometries on the heat transfer surface has been recommended to increase the heat transfer coefficient by several investigators. The use of artificial roughness on the underside of the absorber plate disturbs the viscous sub-layer of the flowing medium. It is well known that in a turbulent flow a sub-layer exists in the flow in addition to the turbulent core. The purpose of the artificial roughness is to make the flow turbulent adjacent to the wall in the sub-layer region. Artificial roughness can be produced by machining, casting, forming, welding and other methods.

Artificial roughness can be produced on a surface by

(i) Blasting sand over it.
(ii) Fixing grooves and ridges.
(iii) Fixing ribs of different geometry such as round, rectangular or V-shaped or Inclined broken ribs, V-shaped discrete ribs etc.
(iv) By fixing wires.
(v) By fixing three dimensional roughness geometries.

The studies on the effect of roughness geometry parameters on the heat transfer and friction factor have been carried out to determine the most efficient configuration and optimum dimensions of the roughness geometry elements. Some of the important geometries and the related parameters that characterize the roughness geometry and substantially influence the performance are given in Table 1.

3. Types of artificial roughness elements investigated

Prasad and Mullick [9] studied the effect of protruding wires on friction factor, heat transfer rate and plate efficiency factor of a solar air heater used for drying of agricultural products. High mass flow rates were used to have turbulent flow in the ducts and protruding wires of 1 mm diameter tripped the laminar sub-layer. They compared the heat transfer, friction factor and plate efficiency factor of roughened corrugated and roughened plane absorber plates with that of corrugated without roughness and smooth absorber plates. The protruding wires enhanced the heat transfer rate for the roughened air heaters and plate efficiency factor improved from 0.63 to 0.72 resulting in 14% improvement in the performance.

Prasad and Saini [10,11] studied the effect of roughness and flow parameters such as relative roughness height, e/D, and relative roughness pitch, P/e, on heat transfer coefficient and friction factor for a fully turbulent flow. They found that the maximum heat transfer occurred in the vicinity of reattachment points and reattachment of free shear layer does not occur if relative roughness pitch, P/e, is less than about 8–10. Optimal thermohydraulic (thermal as well as hydraulic) performance is achieved for roughness height slightly higher than the transition sub layer thickness. For relative roughness height, e/D, value of 0.033 and relative roughness pitch, P/e, value of 10, maximum enhancement in heat transfer rate and friction factor was reported to be 2.38 and 4.25 times respectively in comparison with smooth duct.

Verma and Prasad [12] carried out an outdoor experimental investigation for thermohydraulic (thermal as well as hydraulic) optimization of the roughness geometry and flow parameters for Reynolds number, Re, range of 5000–20,000, relative roughness pitch, P/e, range of 10–40 and relative roughness height, e/D, range of 0.01–0.03. The optimal value of roughness Reynolds number, e^+, was found to be 24 and corresponding to this value, thermohydraulic efficiency parameter value was found to be 71 percent. Heat transfer enhancement factor was found to vary between 1.25 and 2.08 for the range of parameters investigated. Karwa [13] experimentally investigated the effect of repeated rectangular cross-section ribs on heat transfer coefficient and friction factor for duct aspect ratio, W/H, range of 7.19–7.75, relative roughness pitch, P/e, value 10, relative roughness height, e/D, range of 0.0467–0.050, Reynolds number, Re, range of 2800–15000. It was explained that vortices originating from the roughness elements beyond the laminar sub layer are responsible for heat removal as well as increase in pressure drop. The enhancement in the Stanton number was reported to be 65–90% while friction factor was found to be 2.68–2.94 times over smooth duct.

Sahu and Bhagoria [14] experimentally investigated the effect of 90° broken ribs on the enhancement of the thermal performance of solar air heaters for fixed roughness height, e, value of 1.5 mm, duct aspect ratio, W/H, value of 8, pitch, P, in the range of 10–30 mm and Reynolds number, Re, range of 3000–12000.

Table 2
Correlations developed for heat transfer and friction factor for different roughness geometries used in solar air heaters.

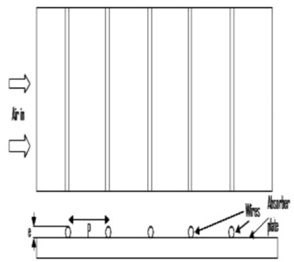
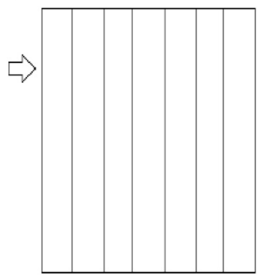
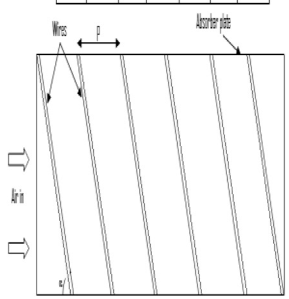
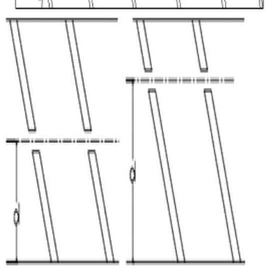
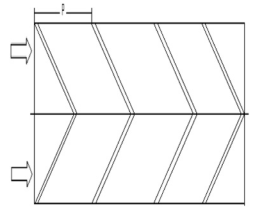
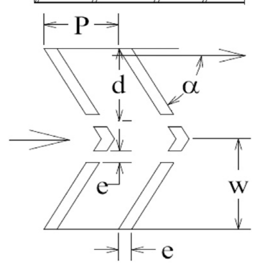
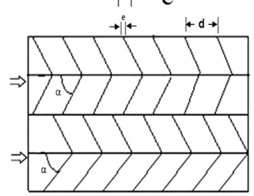
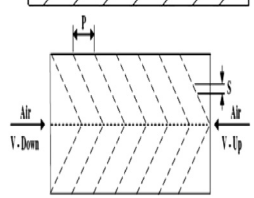
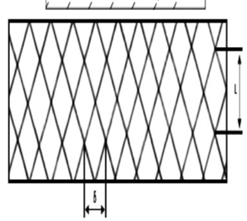
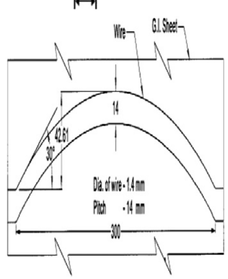
Investigators	Type of roughness	Geometry	Correlation heat transfer coefficient	Correlation friction factor
Prasad and Saini [10]	Transverse wire roughness		$St=\left(\frac{f}{2}\right)/\left[1+\sqrt{\frac{f}{2}}\left\{4.5\ Pr^{0.57}(e^{+})^{0.28}-0.95\left(\frac{P}{2}\right)^{0.53}\right\}\right]$	$f=2/[0.95\ (P/e)^{0.53}+2.4\ \ln(D/2e)-3.75]$
Verma and Prasad [12]	Small dia. Transverse protrusion wire		$Nu_r=0.0859(P/e)^{-0.054}(e/D)^{0.072}Re^{0.723}$ for $e\le 24$	$f_r=0.025(P/2)^{-0.0206}(e/D)^{0.021}Re^{-1.25}$
Gupta et al. [15]	Oblique wire roughness		$Nu=0.00247(e/D)^{0.001}(W/H)^{-0.06}Re^{1.084}$ $\times[\exp\{-0.04(1-\alpha/60^{\circ})^2\}]fore^{+}<35$	$f=0.1991(e/D)^{0.196}(W/H)^{-0.093}Re^{-0.165}\times[\exp\{-0.0993(1-\alpha/70^{\circ})^2\}]$
Aharwal et al. [16]	Inclined rib with gap		$\mathbf{Nu}=0.002(\mathbf{Re})^{1.08}(P/e)^{1.87}\times\mathbf{exp}[-0.45(\mathbf{ln}\ (P/e))^2](\alpha/60)^{0.006}$ $\times\mathbf{exp}[-0.65(\mathbf{ln}\ \alpha/60)^2](d/W)^{-0.32}\times\mathbf{exp}[-0.12(\ln d/W)^2](g/e)^{-0.03}$ $\times\mathbf{exp}[-0.18(\ln g/e)^2](e/D)^{0.5}$	$f=0.071(Re)^{-0.133}(P/e)^{1.83\times}\times\exp[-0.44(\ln(P/e))^2](d/W)^{-0.43}$ $\times\exp[-0.14(\ln d/W)^2](g/e)^{-0.052}\times(\alpha/60)^{0.67}\times\exp[0.12\ (\ln g/e)^2](e/D)^{0.69}$

Table 2 (*continued*)

Investigators	Type of roughness	Geometry	Correlation heat transfer coefficient	Correlation friction factor
Momin et al. [17]	V shaped wire roughness		$Nu=0.067(e/D)^{0.424}Re^{0.888}\times(\alpha/60^\circ)^{-0.077}[\exp\{-0.782(\ln(\alpha/60^\circ))^2\}]$	$f=6.266(e/D)^{0.565}Re^{0.425}\times(\alpha/60^\circ)^{-0.093}[\exp\{-0.719(\ln(\alpha/60^\circ))^2\}]$
Singh et al. [37]	V-shaped with gap		$\mathbf{Nu}=2.36\times10^{-3}\mathbf{Re}^{0.90}(P/e)^{3.50}\times(\alpha/60)^{-0.023}(d/W)^{-0.043}(\mathbf{g}/\mathbf{e})^{-0.014}(e/D)^{0.47}\times\mathbf{exp}(-0.84(\mathbf{ln}(P/e)^2))\mathbf{exp}(-0.72(\mathbf{ln}(\alpha/60)^2))\times\mathbf{exp}(-0.05(\mathbf{ln}(d/W)^2))\mathbf{exp}(-0.15(\mathbf{ln}(g/e)^2))$	$f=4.13\times10^{-2}Re^{-0.126}(P/e)^{2.74}(\alpha/60)^{-0.034}(d/W)^{-0.058}\times(g/e)^{0.031}(e/D)^{0.70}\exp(-0.685(\ln(P/e)^2))\times\exp(-0.93(\ln(\alpha/60)^2))\times\exp(-0.058(\ln(d/W)^2))\exp(-0.21(\ln(g/e)^2))$
Kumar et al. [27]	Discrete W-shaped ribs		$Nu=0.105\times(Re)^{0.873}\times\left(\frac{e}{D}\right)^{0.453}\times\left(\frac{\alpha^\circ}{60}\right)^{-0.081}\times\exp\left[-0.59\times\left(\ln\left(\frac{\alpha^\circ}{60}\right)\right)^2\right]$	$f=5.68\times(Re)^{-0.40}\times(e/D)^{0.59}\times\left(\frac{\alpha^\circ}{60}\right)^{-0.081}\times\exp\left[-0.57\times\left(\ln\left(\frac{\alpha^\circ}{60}\right)\right)^2\right]$
Hans et al., [8]	V-shaped discrete		$Nu=0.0054Re^{1.29}\times\left(\frac{B}{S}\right)^{1.34}\left(\frac{S'}{S}\right)^{1.112}\left(\frac{e}{D}\right)^{0.27}\left(\frac{P'}{P}\right)\Big)^{2}\Big]\times\exp\left[-0.376\left(\ln\left(1-\left(\frac{\alpha}{60}\right)\right)\right)^2\right]$	$f=0.717Re^{-2.991}\times\left(\frac{B}{S}\right)^{0.0636}\left(\frac{S'}{S}\right)^{0.0712}\times\left(\frac{e}{D}\right)^{0.113}\left(\frac{P'}{P}\right)^{-0.0093}\times\exp\left[-1.26\left(\ln\left(1-\left(\frac{\alpha}{70}\right)\right)\right)^2\right]$
Hans et al. [8]	Expanded metal mesh		$Nu=4\times10^{-4}Re^{1.22}(e/D)^{0.625}\times(S/10e)^{2.22}(L/10e)^{2.66}\times[\exp\{-1.25(\ln(S/10e))^2\}]\times[\exp\{-0.824\ln(L/10e)^2\}]$	$f=0.815\,Re^{-0.361}(L/e)^{0.266}\times(S/10e)^{-0.19}(10e/D)^{0.591}$
Saini and Saini [22]	Arc shaped rib		$\mathbf{Nu}=0.001047\mathbf{Re}^{1.3186}(\mathbf{e}/\mathbf{D})^{0.3772}\times(\alpha/90)^{-0.1198}$	$f=0.14408Re^{-0.17103}(e/D)^{0.1765}\times(\alpha/90)^{0.1185}$

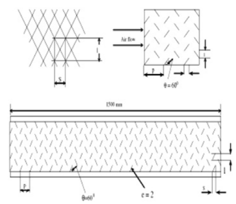
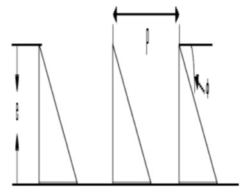
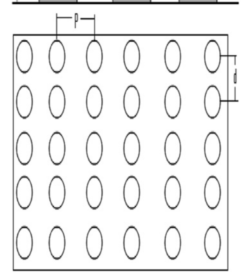
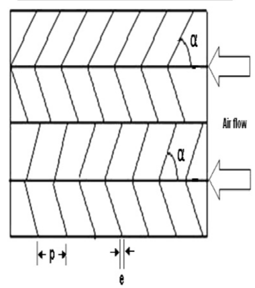
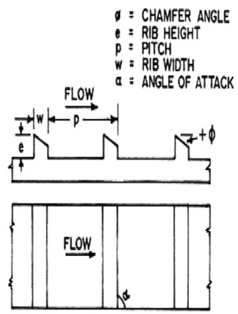
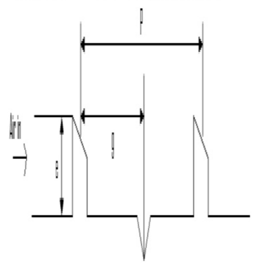
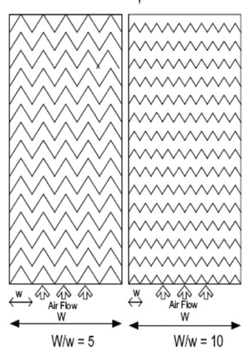
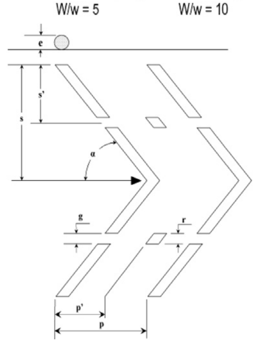
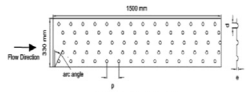
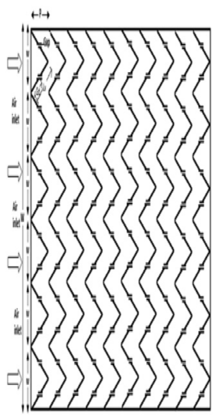
Karmare and Tikekar [23]	Metal grit rib		$\mathbf{Nu} = 2.4\times10^{-3}\times \mathbf{Re}^{1.3}\times(e/D)^{0.42}(\mathbf{l/s})^{-0.146}\times(P/e)^{-0.27}$	$f=15.55\times Re^{-0.263}\times(e/D)^{0.91}(l/s)^{-0.27}\times(P/e)^{-0.51}$
Bhagoria et al. [24]	Wedge rib roughness		$Nu=1.89\times10^{-4}(e/D)^{0.426}Re^{1.21}(P/e)^{2.94}\times[\exp(-0.71\ln(P/e))^2](\Phi/10)^{-0018}[\exp\{-1.50(\ln(\phi/10^\circ))^2\}]$	$f=12.44\times(e/D)^{0.99}\times Re^{-0.18}\times(P/e)^{-0.52}\times(\alpha/10^\circ)^{0.49}$
Saini and Verma [25]	Dimple shape rib		$Nu=5.2\times10^{-4}Re^{1.27}\{(P/e)^{3.15}\}\times[\exp(-2.12)(\log(P/e))^2](e/D)^{0.033}\times[\exp(-1.3)(\log(e/D))^2]$	$f=0.642\,Re^{0.423}(P/e)^{-0.465}\times[\exp(0.054)(\log(P/e))^2](e/D)^{-0.0214}\times[\exp(0.84)(\log(e/D))^2]$
Kumar et al. [27]	Discrete Wshaped ribs		$Nu_r=0.105\times(Re)^{0.873}\times(e/Dh)^{0.453}\times(\alpha/60^\circ)^{-0.081}\times\exp[-.59\times(\ln(\alpha/60^\circ))^2]$	$f_r=5.68\times(Re)^{-0.40}\times(e/Dh)^{0.59}\times(\alpha/60^\circ)^{-0.081}\times\exp[-0.579\times(\ln(\alpha/60^\circ))^2]$
Layek et al. [29]	Chamfered rib-grooved		$Nu=0.00225\times Re^{0.92}(e/D)^{0.52}(P/e)^{1.72}\times\exp[-0.22(\ln\varnothing)^2]\times\exp[-0.46\{\ln(P/e)\}^2](g/P)^{-1.21}\varnothing^{1.24}\times\exp[-0.74\{\ln(g/P)\}^2]$	$f=0.00245\times Re^{0.124}(e/D)^{0.365}(P/e)^{4.32}(g/P)^{-1.124}\times\exp[-1.09\{\ln(P/e)\}^2]\times\exp[-0.68\{(g/P)\}^2]\times\exp[0.005\varnothing]$

Table 2 (*continued*)

Investigators	Type of roughness	Geometry	Correlation heat transfer coefficient	Correlation friction factor
				
Jaurker et al. [30]	Rib groove-compound roughness		$Nu = 0.00206\,Re^{0.936}(e/D)^{0.349}(P/e)^{3.318}$ $\times\exp[-0.868\{\ln(P/e)\}^2](g/P)^{1.108}$ $\times\exp[2.486\{\ln(g/P)\}^2+1.405\{\ln(g/P)\}^3]$	$f = 0.00127\,Re^{-0.199}(e/D)^{0.585}(P/e)^{7.19}$ $\times(g/P)^{0.645}\times\exp[-1.854\{\ln(P/e)\}^2]$ $\times\exp[1.513\{\ln(g/P)\}^2+0.8662\{\ln(g/P)\}^3]$
Hans et al. [32]	Continuous Multi v-rib		$Nu = 3.35\times10^{-5}Re^{0.92}(e/D)^{0.77}\times(W/w)^{0.43}(\alpha/90)^{-0.49}$ $\times\exp(0.117\ln(W/w)^2)$ $\times\exp(-0.61\ln(\alpha/90)^2)(P/e)^{-8.54}$ $\times\exp(-2.0407\ln(P/e)^2)$	$f = 4.47\times10^{-4}Re^{-0.3188}(e/D)^{-0.73}$ $\times(W/w)^{-0.22}(\alpha/90)^{-0.39}\exp(0.52\ln(\alpha/90)^2)\times(P/e)^{8.9}\exp(2.133\ln(P/e)^2)$
Patil et al. [56–58]	Discrete v-rib with Combined staggered rib pieces		$Nu = 0.0089\,Re^{0.97}$ $\times\exp\left[\frac{0.12}{1}+\{2.42\ln(\frac{s'}{s})+1.19\}^2+0.11/1+\{2.5\ln(p'/p)+1.41\}^2\right]$ $+0.14[\ln(r/e)]^{0.71}$	$f = 0.09Re^{-0.18}$ $\times\exp\left[\frac{0.10}{1}+\{3.18\ln(\frac{s'}{s})+1.56\}^2+0.08/1+\{2.61\ln(p'/p)+1.40\}^2\right]$ $+0.17\{\ln(r/e)^{2.5}\}$

Sethi et al. [59]	Dimpled shaped	 (a) Diagram of the absorber plate  (b) Pictorial view of the absorber plate	$Nu = 7.1 \times 10^{-3} \times (e/D)^{0.362} \times (P/e)^{-0.047} \times (\alpha/60)^{-0.0048} \times \exp[-0.7792(\ln(\alpha/60))^2]$	$f = 4.869 \times 10^{-1}(e/D)^{0.2663} \times Re^{-0.223} \times (P/e)^{-0.059} \times (\alpha/60)^{0.0042} \times \exp[-0.4801(\ln(\alpha/60))^2]$
Kumar et al. [61]	Multi v-shaped with gap rib		$Nu = 8.532 \times 10^{-3}(Re)^{0.932}\left(\frac{\mathbf{g}}{\mathbf{D}}\right)^{0.175}\left(\frac{W}{w}\right)^{0.506} \times \left[\exp\left(-0.0753\left(Ln\left(\frac{W}{w}\right)\right)^2\right]\left(\frac{G_d}{L_v}\right)^{-0.0348} \times \left[\exp\left(-0.0653\left(Ln\left(\frac{G_d}{L_v}\right)\right)^2\right]\left(\frac{g}{e}\right)^{-0.0708} \times \left[\exp\left(-0.223\left(Ln\left(\frac{g}{e}\right)\right)^2\right] \times \left(\frac{\alpha}{60}\right)^{-0.0239}\left[\exp\left(0.1153\left(Ln\left(\frac{\alpha}{60}\right)\right)^2\right] \times \left(\frac{p}{e}\right)^{1.196}\left[\exp\left(-0.2805\left(Ln\left(\frac{p}{e}\right)\right)^2\right]$	$f = 3.1934\,(Re)^{-0.3151}\left(\frac{e}{D}\right)^{0.268}\left(\frac{W}{w}\right)^{0.1132} \times \left[\exp\left(0.0974\left(Ln\left(\frac{W}{w}\right)\right)^2\right]\left(\frac{G_d}{L_v}\right)^{0.0610} \times \left[\exp\left(-0.1065\left(Ln\left(\frac{G_d}{L_v}\right)\right)^2\right]\left(\frac{g}{e}\right)^{-0.1769} \times \left[\exp\left(-0.6349\left(Ln\left(\frac{g}{e}\right)\right)^2\right] \times \left(\frac{\alpha}{60}\right)^{0.1553}\left[\exp\left(-0.1527\left(Ln\left(\frac{\alpha}{60}\right)\right)^2\right] \times \left(\frac{p}{e}\right)^{-0.7941}\left[\exp\left(0.1486\left(Ln\left(\frac{p}{e}\right)\right)^2\right]$

Roughened heated plate increased the heat transfer coefficient by 1.25–1.4 times as compared to smooth rectangular duct under similar operating conditions. Corresponding to roughness pitch, *P*, value of 20 mm, maximum value of heat transfer was obtained that decreased on the either side of this roughness pitch, *P*, value. Based on the experimental investigation, the thermal efficiency of roughened solar air heater was found to be in the range of 51–83.5% depending upon the flow conditions.

Gupta et al. [15] studied the effect of relative roughness height (e/D), inclination of rib with respect to flow direction (α) and Reynolds number, Re, on the thermohydraulic performance of a roughened solar air heater for transitionally rough flow region ($5 < e^{+} < 70$). For a roughened solar air heater, maximum enhancement in Nusselt number and friction factor was reported to be of the order 1.8 and 2.7 times respectively corresponding to angle of inclination values of 60° and 70°, respectively. Best thermohydraulic (thermal as well as hydraulic) performance was reported for relative roughness height (e/D) value of 0.023 and Reynolds number, Re, value of 14,000.

Aharwal et al. [16] experimentally studied the effect of width and position of gap in an inclined discrete ribs having square cross-section on heat transfer and friction characteristics of a rectangular duct. The duct had an aspect ratio, W/H, of 5.84, relative roughness pitch, P/e, of 10, relative roughness height, e/D, of 0.0377, angle of attack, α, of 60°, relative gap width, g/e, range of 0.5–2 and relative gap position, d/W, varied from 0.1667 to 0.667 for Reynolds number, Re, range of 3000–18000. For the discrete ribs and continuous rib roughened ducts, the enhancement in heat transfer was reported to be in the range of 1.71–2.59 times and 1.48–2.26 times respectively under similar operating conditions. The maximum values of heat transfer ratio (Nu/Nu_s), friction factor ratio (f/f_s) and thermohydraulic parameter obtained were corresponding to relative gap width (g/e) value of 1.0 and relative gap position (d/W) value of 0.25 for the range of parameters investigated. Particle Image Velocimetry (PIV) system was used to visualize the effects of rib geometry on the flow behaviour.

Momin et al. [17] experimentally investigated the effect of geometrical parameters of v-shaped ribs on heat transfer and friction factor characteristics of a rectangular duct of a solar air heater. The investigation covered a Reynolds number, Re, range of 2500–18000, relative roughness height, e/D, range of 0.02–0.034 and angle of attack, α, range of 30 degree–90° for a fixed relative roughness pitch, P/e, of 10. Rate of increase of Nusselt number was observed to be lower than the rate of increase of friction factor with an increase in Reynolds number. The maximum enhancement of heat transfer and friction factor as a result of providing artificial roughness had been found to be 2.30 and 2.83 times respectively over the smooth duct for an angle of attack, α, value of 60°. It was reported that for relative roughness height, e/D, value of 0.034 and angle of attack, α, value of 60°, v-shaped ribs enhanced the value of Nusselt number by 1.14 and 2.30 times over inclined ribs and smooth absorber plate respectively.

Varun et al. [18] carried out a comparative experimental study of augmented heat transfer and friction in a rectangular duct having rectangular cross-section ribs arranged in transverse, inclined, v-shaped continuous and v-shaped discrete pattern for duct aspect ratio, W/H, range of 7.19–7.75, relative roughness pitch, P/e, value 10, relative roughness height, e/D, range of 0.0467–0.050 and Reynolds number, Re, range of 2800–15000. The enhancement in the Stanton number over the smooth duct was reported to be in range of 65–90%, 87–112%, 102–137%, 110–147%, 93–134% and 102–142% for transverse, inclined, v-shaped up continuous, v-shaped down continuous, v-shaped up discrete and v-shaped down discrete rib arrangement respectively. The friction factor ratios corresponding to these arrangements were found as 2.68–2.94, 3.02–3.42, 3.40–3.92, 3.32–3.65, 2.35–2.47 and 2.46–2.58 respectively

Karwa et al.[19] experimentally studied the heat transfer and friction in a high aspect ratio, W/H, rectangular duct with repeated rectangular cross-section ribs on one broad wall in v-shaped discrete and discontinuous patterns at angles of inclination of 45° and 60°, relative roughness pitch, P/e, value of 10.63, relative roughness length, B/S, values 3 and 6 with Reynolds number, Re, varied from 2850 to 15500. It was observed that corresponding to relative roughness length, B/S, value of 6, the highest and the lowest values of Stanton number ratio, St/St_s, were obtained for 60° v-shaped down discrete and 60° v-shaped up discontinuous ribs respectively. Friction factor ratio, f/f_s, values were found to be maximum and minimum for 60° v-shaped down discrete and 45° v-shaped up discrete ribs corresponding to relative roughness length, B/S, value of 3. Stanton number and friction factor values were reported to be higher for v-shaped down pattern in comparison with v-shaped up pattern and 60° v-shaped ribs performed better than the 45° v-shaped ribs. Rib pattern had a strong effect on the Stanton number and friction factor with discrete ribs performing better than other rib configurations from thermohydraulic performance point of view.

Karwa et al. [20] performed an experimental investigation of Nusselt number and friction factor for rectangular ducts, having aspect ratio, W/H, in the range of 4.8–12, and roughened with repeated integral chamfered ribs. The roughness geometry and flow parameters considered for the investigation were Reynolds number, Re, range of 3000–20000, relative roughness height, e/D, range of 0.014–0.0328, relative roughness pitch, P/e, range of 4.5–8.5 and chamfer angle, Φ, varying from $-15°$ to 18°. Stanton number and friction factor increased with increase in chamfer angle and attained maximum value corresponding to chamfer angle, Φ, and value of 15°. It was reported that Stanton number decreased while friction factor increased with increase in aspect ratio, W/H. As compared to the smooth solar air heater duct, the presence of chamfered ribs on one of the broad wall of duct yielded up to about two-fold and three-fold increase in the Stanton number and the friction factor respectively in the range of parameters investigated.

Saini and Saini [21] carried out an experimental investigation to study the effect of wire mesh roughened absorber plate on Nusselt number augmentation and friction factor characteristics of solar air heaters. The investigation considered relative longway length of mesh, L/e, in range of 25–71.87, relative shortway length of mesh, S/e, in range of 15.62–46.87, relative roughness height, e/D, in range of 0.012–0.039 and Reynolds number, Re, in range of 1900–13000. It was reported that the maximum heat transfer of order 4 times over the smooth duct were obtained corresponding to angle of attack of 61.9°, relative longway length of mesh, L/e, value of 46.87 and relative shortway length of mesh, S/e, value of 25. Maximum value of friction factor was reported for angle of attack of 72°, relative longway length of mesh, L/e, value of 71.87 and relative shortway length of mesh, S/e, value of 15. Saini and Saini [22] studied the effect of arc shaped ribs on the Nusselt number and friction factor of rectangular ducts with Reynolds number, Re, relative roughness height, e/D, and relative arc angle, α, varying from 2000 to 17000, 0.0213 $-$0.0422 and 0.3333–0.6666 respectively. It was reported that relative arc angle, α, had an opposite effect on Nusselt number enhancement and friction factor. With decrease in relative arc angle, α, value, Nusselt number value increased while friction factor value decreased. Enhancement of Nusselt number and friction factor was reported to be of order 3.6 and 1.75 times respectively over smooth solar air heater duct for relative arc angle, α, value of 0.3333 and relative roughness height, e/D, value of 0.0422.

Karmare and Tikekar [23] experimentally investigated the heat transfer coefficient and friction factor characteristics of a rectangular duct having absorber plate roughened with defined grid of metal ribs of circular cross-section and the investigated roughness geometry. The investigation considered relative roughness height,

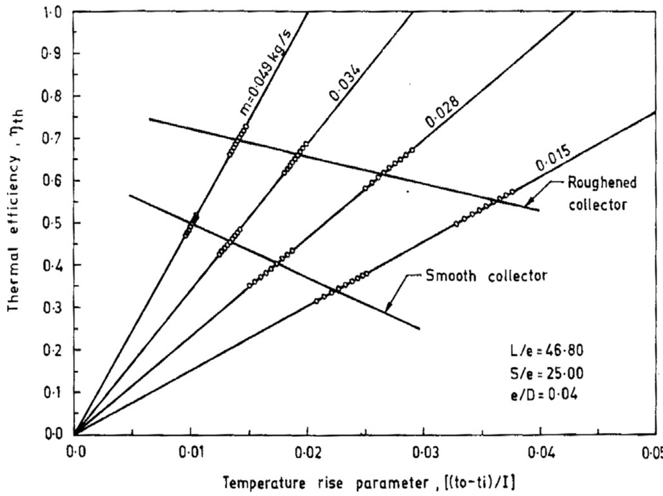


Fig. 1. Thermal performance of solar air heater with absorber plates [35].

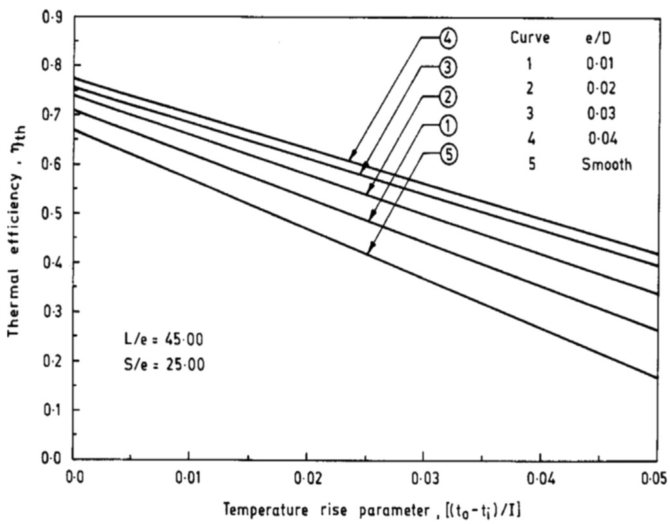


Fig. 2. Effect of relative roughness height (e/D) on thermal performance [35].

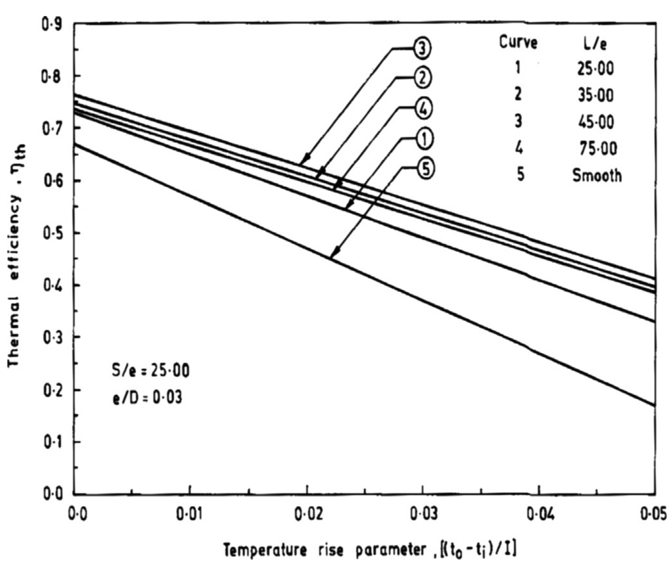


Fig. 3. Effect of relative roughness height (L/e) on thermal performance [35].

e/D, range of 0.035–0.044, relative roughness pitch, P/e, range of 12.5–36, relative grit length, l/s, range of 1.72–1 and Reynolds number, Re, range of 4000–17,000. Enhancement in heat transfer

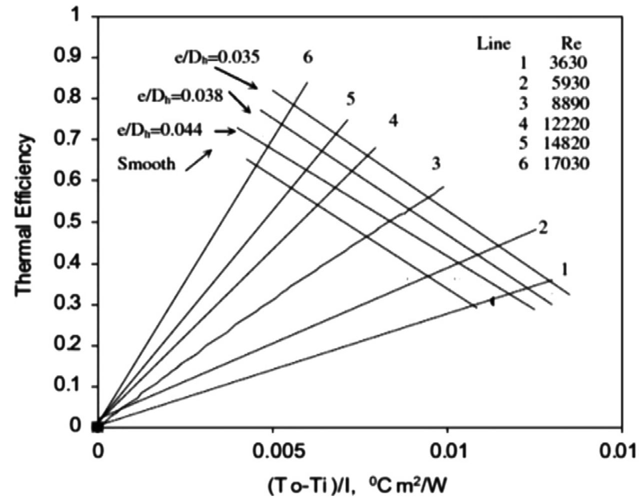


Fig. 4. Thermal efficiency versus thermal performance for different value of Re and e/D [36].

rate was found to be 187% and the friction factor increased by 213% and optimum performance was observed for relative grit length, l/s, value of 1.72, relative roughness height, e/D, value of 0.044, and relative roughness pitch, P/e, value of 17.5 for the range of parameters studied. Bhagoria et al. [24] experimentally studied heat transfer and fluid flow characteristics in a solar air heater with absorber plate roughened with wedge shaped transverse integral ribs. The investigation encompassed the Reynolds number, Re, range of 3000–18000, relative roughness height, e/D, range of 0.015–0.033 and rib wedge angle, Φ, range of 8–12°. It was reported that heat transfer rate and friction factor increased by 2.4 and 5.3 times over smooth duct in the range of parameters investigated.

Saini and Verma [25] studied the effect of roughness geometry and operating parameters on heat transfer coefficient and friction factor in a roughened duct provided with dimple-shape roughness geometry for the range of Reynolds number, Re, from 2000 to 12,000, relative roughness height, e/D, from 0.018 to 0.037 and relative roughness pitch, P/e, from 8 to 12. For the range of parameters investigated, Nusselt number was found to be maximum corresponding to relative roughness height, e/D, of 0.0379 and relative roughness pitch, P/e, of 10. For fixed value of relative roughness pitch, P/e, of 10, friction factor attained the maximum and minimum values corresponding to relative roughness height, e/D, values of 0.0289 and 0.0189 respectively. Lanjewar et al. [26] investigated the heat transfer and friction characteristics of artificially roughened ducts with W-shaped ribs. The range of parameters for this study has been decided on the basis of practical considerations of the system and operating conditions. The duct has a width to height ratio (W/H) of 8.0, relative roughness pitch (P/e) of 10, relative roughness height (e/D_h) of 0.03375 and angle of attack of flow (α) of 30–75°. The heat transfer and friction factor results have been compared with those for smooth duct under similar flow and thermal boundary condition and thermo-hydraulic performance has been investigated.

Kumar and Bhagoria [27] studied heat transfer and friction characteristics of a rectangular channel having discrete w-shaped rib roughness. The experiment encompassed the Reynolds number, Re, range from 3000–15000, relative roughness height, e/D, range from 0.0168–0.0337, relative roughness pitch, P/e, value 10, and angle of attack, α, range from 30°–75°. It was reported that maximum enhancement of Nusselt number and friction factor in comparison to smooth duct was of order of 2.16 and 2.75 times respectively for an angle of attack, α, value of 60°. Flow separation and secondary flow resulting due to the presence of discrete

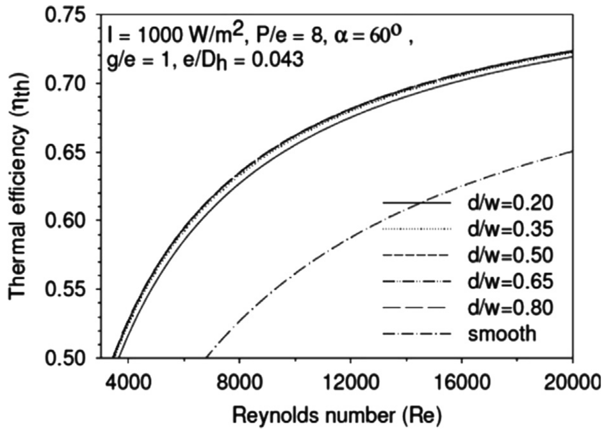


Fig. 5. Thermal efficiency as a function of Reynolds number and relative gap position [37].

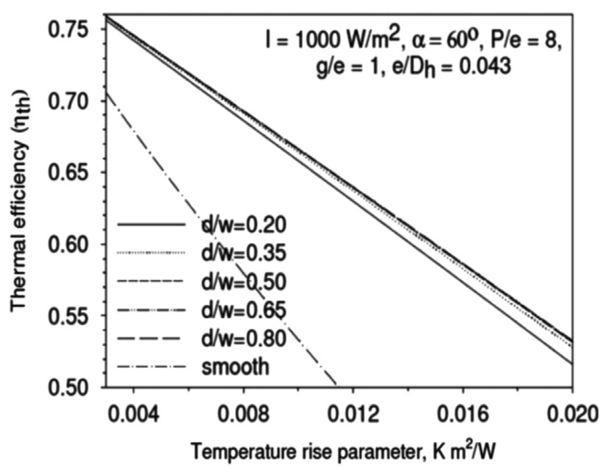


Fig. 6. Thermal efficiency as a function of temperature rise parameter and relative gap position [37].

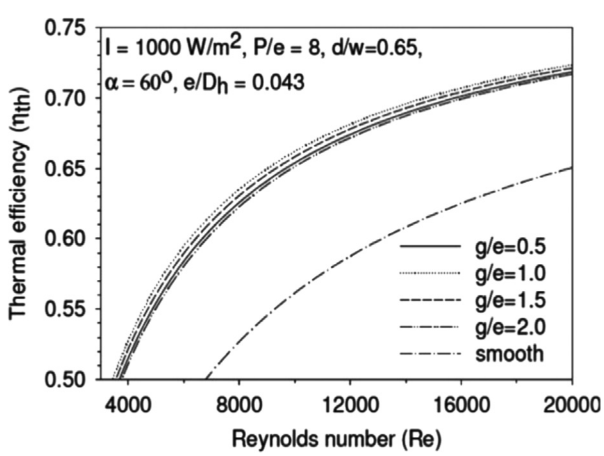


Fig. 7. Thermal efficiency as a function of Reynolds number and relative gap width [37].

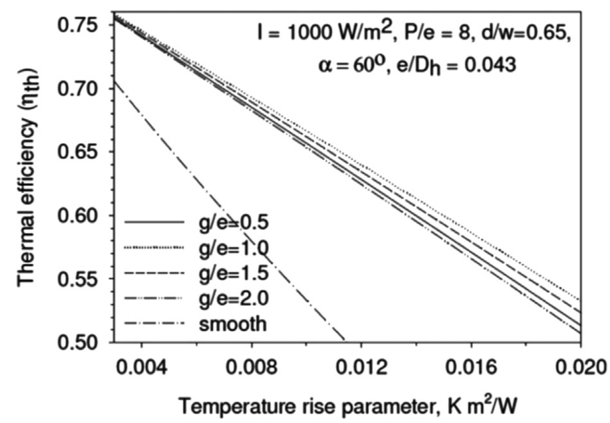


Fig. 8. Thermal efficiency as a function of temperature rise parameter and relative gap width [37].

w-shaped rib combined to provide an optimum value of angle of attack, α.

Varun et al. [28] carried out an experimental study on heat transfer coefficient and friction factor characteristics by using a combination of inclined and transverse ribs on the heated plate of a solar air heater with Reynolds number, Re, ranging from 2000 to 14 000, relative roughness pitch, P/e, range of 3–8, relative roughness height, e/D, value of 0.030, duct aspect ratio, W/H, value of 10 and roughness height, e, value of 1.60 mm. For relative roughness pitch, P/e, value of 8, the best thermal performance was reported. Layek et al.[29] carried out an experimental investigation to study the heat transfer coefficient and friction factor for repeated transverse compound rib-groove arrangement on heated plate of a solar air heater. Four relative rib-groove positions, g/P, values of 0.3, 0.4, 0.5 and 0.6 were investigated for fixed relative roughness height, e/D, and relative roughness pitch, P/e, values of 0.030 and 10 respectively. It was found that relative roughness pitch, P/e, value of 10, relative groove position, g/P, value of 0.4 provided about 2.42 and 2.6 times increase in the Nusselt number and friction factor respectively for entire range of Reynolds number, Re, studied.

Jaurker et al. [23] experimentally investigated the heat transfer and fluid flow characteristics of rib-groove roughened rectangular duct. The effect of relative roughness pitch, P/e, relative roughness height, e/D and relative groove position, g/P, on heat transfer coefficient and friction factor has been studied. The presence of rib-grooved artificial roughness enhanced Nusselt number and friction factor up to 2.70 and 3.60 times respectively in comparison to smooth absorber plate. The maximum heat transfer rate occurred for a relative roughness pitch, P/e, of about 6 and relative groove, g/P, value of 0.4. Bopche and Tandale [31] carried out an experimental investigation to study the heat transfer coefficient and friction factor of a rectangular duct roughened artificially with U-shaped turbulator. The experimental encompassed Reynolds number, Re, range from 3800 to 18000, ratio of turbulator height to hydraulic mean diameter, e/D, is varied from 0.0186 to 0.03986, relative roughness pitch, P/e, range of 6.67 to 57.14 and value of angle of attack, α, is kept constant at 90 degree. The U-shaped roughness geometry shows appreciable heat transfer enhancement even when Reynolds number value is less than 5000 where ribs are generally inefficient. At Reynolds number value of 3800, maximum enhancement in Nusselt number and friction factor are reported to be 2.388 and 2.50 respectively.

Hans et al. [32] investigated heat transfer coefficient and friction factor characteristics of Multiple v-shaped ribs roughened rectangular duct. The investigation encompassed Reynolds number, Re, from 2000 to 20000, relative roughness height (e/D) values of 0.019–0.043, relative roughness pitch (P/e) range of 6–12,angle of attack (α) range of 30°–75° and relative roughness width (W/w) range 1–10. Based on the experimental results, correlations for heat transfer coefficient and friction factor were developed. A maximum enhancement of heat transfer rate and friction factor due to presence of such an artificial roughness has been found to be 6 and 5 times, respectively, in comparison to the smooth duct for the range of parameters considered. The maximum heat

Table 3
Relative performances of rough tubes [39].

Case	Description	Constraints	Parameter	Relative mass velocity (G^*)
1	Reduced surface area	$\frac{P}{P_s}=\frac{Q}{Q_s}=1$	$\frac{A}{A_s}=\frac{(f/f_s)^{0.5}}{(\mathrm{St}/\mathrm{St}_s)^{1.5}}$	$G^*=\frac{(f/f_s)^{0.5}}{(\mathrm{St}/\mathrm{St}_s)^{0.5}}$
2	Increased heat transfer	$\frac{P}{P_s}=\frac{A}{A_s}=1$	$\frac{K}{K_s}=\frac{(\mathrm{St}/\mathrm{St}_s)}{\sqrt[3]{(f/f_s)}}$	$G^*=(f/f_s)^{1/3}$
3	Reduced pumping power	$\frac{Q}{Q_s}=\frac{A}{A_s}=1$	$\frac{P}{P_s}=\frac{(f/f_s)}{\sqrt[3]{(\mathrm{St}/\mathrm{St}_s)}}$	$G^*=(\mathrm{St}/\mathrm{St}_s)$

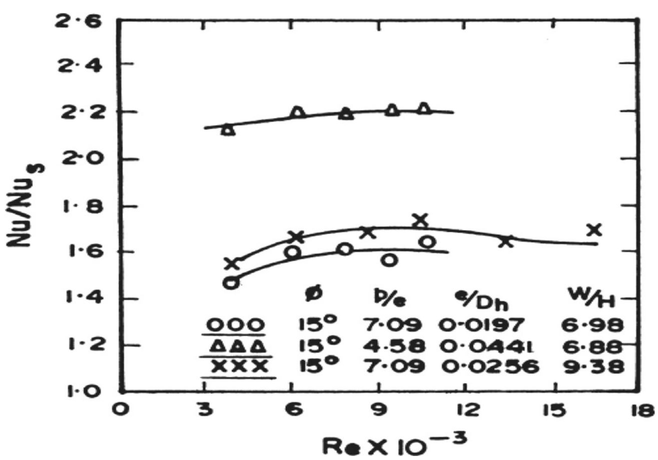


Fig. 9. Nusselt number ratio versus Reynolds number [42].

transfer enhancement has been found to occur for a relative roughness width (W/w) value 6 while friction factor attains maximum value for relative roughness width (W/w) value of 10.

Kumar et al. [60,61] experimentally investigated Nusselt number and friction factor characteristics of Multiple v-shaped with gap ribs roughened rectangular duct. The investigation encompassed Reynolds number, Re, from 2000 to 20000, relative roughness height (e/D) values of 0.022–0.043, relative roughness pitch (P/e) range of 8–12, angle of attack (α) range of 30°–75°, relative gap distance (G_d/L_v) range of 0.24–0.80, relative gap width (g/e) range of 0.5–1.5 and relative roughness width (W/w) range 1–10.

4. Heat transfer and friction factor correlations

In most of the solar air heaters roughened artificially for heat transfer enhancement, correlations have been developed for heat transfer coefficient and friction factor in terms of roughness geometry parameters. Some of the correlations developed for heat transfer coefficient and friction factor are given in Table 2.

5. Thermal performance of solar air heater

It was pointed out earlier that the low thermal efficiency of solar air heaters can be improved by using artificial roughness in the form of different shapes fabricated in various arrangements to create turbulence near the wall or to break the viscous sub layer. As a result, increasing the heat transfer coefficient, thermal efficiency can be increased but at the same time creating turbulence requires additional energy which has to be supplied by fan or blower at the expense of electrical energy.

5.1. Thermal performance representation

The widely used method of performance presentation given by National Bureau of Standard (NBS) and the American Society of Heating, Refrigeration and Air Conditioning Engineering [33].

The collector efficiency, η, is a measure of the collector performance and is defined as the ratio of the useful heat energy gain over a time period to the incident solar radiation over the same time period.

$$\eta=\frac{\int Q_u dt}{A_P \int HRdt} \quad (1)$$

where,

H is the rate of radiation intensity on unit area of surface of any orientation,
R is the factor to convert radiation to that on the plane of the collector.

The instantaneous rate of useful energy collection is the difference between the energy due to incident solar radiation that is absorbed by the absorber plate and the rate at which the energy is lost due to the difference of the plate and the ambient temperatures. The useful energy collected in a solar air heater can be expressed mathematically as

$$Q_u=A_P[I(\tau\alpha)-U_L](T_P-T_a)] \quad (2)$$

To overcome the difficulty of determining the average plate temperature, T_P, a parameter called plate efficiency or collector efficiency factor, F', is introduced. It is defined as

$$F'=\frac{\text{Actual useful energy collected}}{\text{Useful energy collected if entire collector surface were maintained at average fluid temperature}} \quad (3)$$

So it would be convenient to express Eq. (2) in terms of inlet or average fluid temperatures, by introducing the collector efficiency factor, F'as follows:

$$Q_u=F'A_P[I(\tau\alpha)-U_L](T_f-T_a)] \quad (4)$$

where

$$T_f=\frac{(T_o+T_i)}{2} \quad (5)$$

For collector without recycling, $T_a=T_i$, the Eq. (4) reduces to

$$Q_u=F'A_P[I(\tau\alpha)-U_L](T_o-T_i)/2] \quad (6)$$

The rate of useful energy collected is also expressed by considering enthalpy rise of the air as

$$Q_u=mC_P(T_o-T_i) \quad (7)$$

Thermal efficiency can, now be expressed as

$$\eta_{\mathrm{th}}=\frac{Q_u}{IA_P} \quad (8)$$

Then the efficiency of the flat plate collector can be alternatively expressed as:

$$\eta_{\mathrm{th}}=F'[(\tau\alpha)-U_L](T_o-T_i)/2I] \quad (9)$$

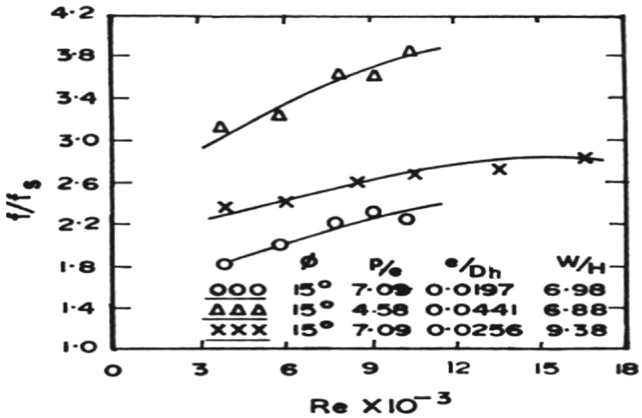


Fig. 10. Friction factor ratio versus Reynolds number [42].

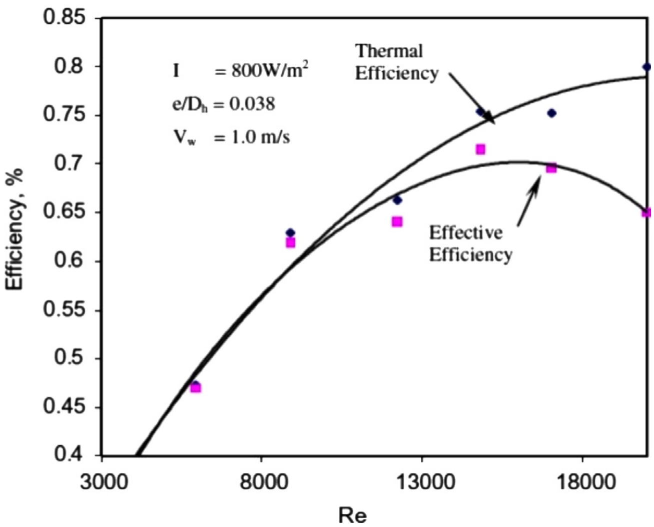


Fig. 11. Efficiency versus Reynolds number [36].

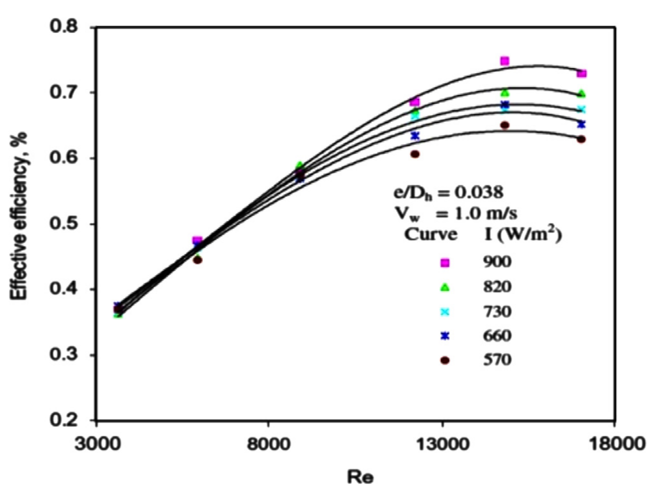


Fig. 12. Variation of effective efficiency at different Reynolds number and Insolation [36].

$$\eta_{\text{th}} = F_P[(\tau\alpha) - U_L](T_o - T_a)/2I] \tag{10}$$

$$\eta_{\text{th}} = mC_P(T_o - T_i)/IA_P] \tag{11}$$

The thermal efficiency of a solar collector can also be expressed in terms of another factor called the heat removal factor, F_o, as

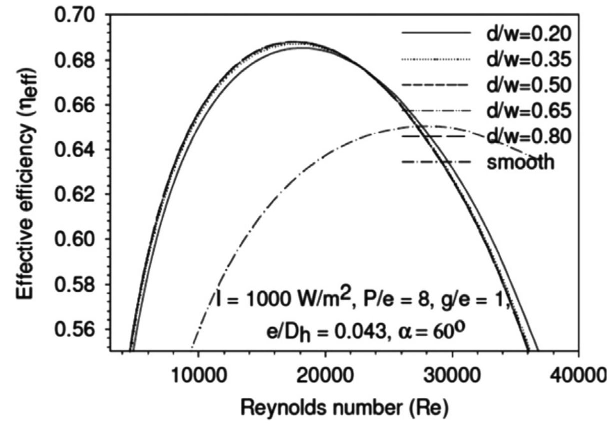


Fig. 13. Effective efficiency as a function of Reynolds number and relative gap position [37].

follows:

$$\eta_{\text{th}} = F_o\left[(\tau\alpha) - U_L\left(\frac{T_i - T_a}{I}\right)\right] \tag{12}$$

Here F_o the collector heat removal factor is defined as the ratio of the actual heat transfer to the maximum possible heat transfer rate when the absorber plate is at the inlet fluid temperature. The quantity F_o is equivalent to the effectiveness of a conventional heat exchanger, which is defined as the ratio of the actual heat transfer to the maximum possible heat transfer. The maximum possible useful energy gain (heat transfer) in a solar collector occurs when the whole collector is at the inlet fluid temperature; heat losses to the surroundings are then at minimum. The collector heat removal factor times this maximum possible energy gain is equal to the actual useful energy gain Q_u.

$$Q_u = F_o A_P[I(\tau\alpha) - U_L](T_i - T_a)] \tag{13}$$

The relation between the collector efficiency factor F' and heat removal factor F_o is given as

$$F_o = \frac{mC_P}{A_P U_L}\left[\exp\left\{\frac{F' U_L A_P}{mC_P}\right\} - 1\right] \tag{14}$$

In particular case of solar air heaters without recycling and where the inlet air temperature coincides the ambient temperature (i.e. $T_i = T_a$), Eq. (12) reduces to

$$\eta = F_o(\tau\alpha) \tag{15}$$

This expression of efficiency does not allow the real operative parameters to be shown.

In view of these limitations, Biondi et al. [34] proposed the following equation for efficiency of solar air heaters, taking in air at ambient temperature ($T_i = T_a$), which is utilized for representing thermal performance:

$$\eta_{th} = F_o\left[(\tau\alpha) - U_L\left(\frac{T_o - T_i}{I}\right)\right] \tag{16}$$

where F_o is the heat removal factor related to outlet temperature and can be expressed as

$$F_o = \frac{mC_P}{A_P U_L}\left[\exp\left\{\frac{F' U_L A_P}{mC_P}\right\} - 1\right] \tag{17}$$

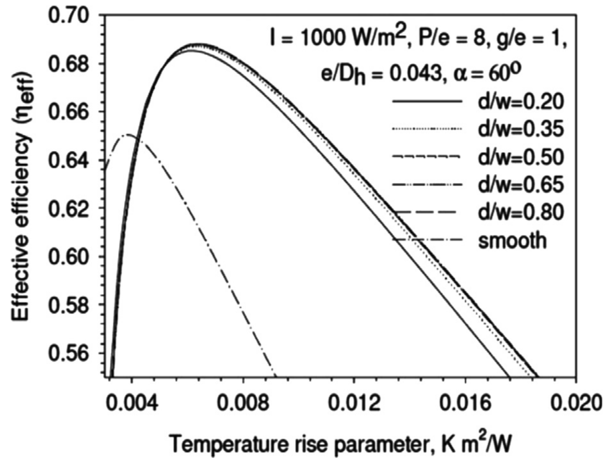


Fig. 14. Effective efficiency as a function of temperature rise parameter and relative gap position [37].

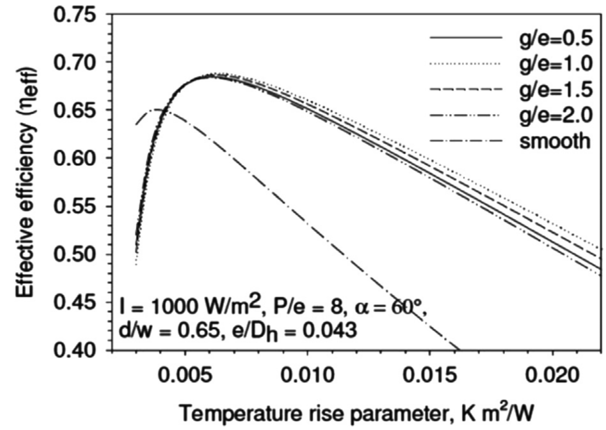


Fig. 16. Effective efficiency as a function of temperature rise parameter and relative gap width [37].

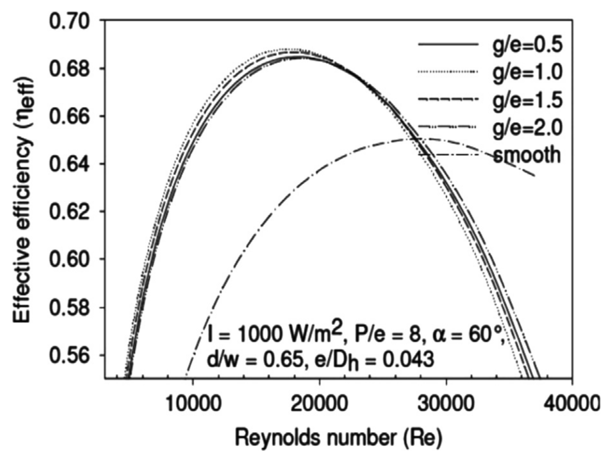


Fig. 15. Effective efficiency as a function of Reynolds number and relative gap width [37].

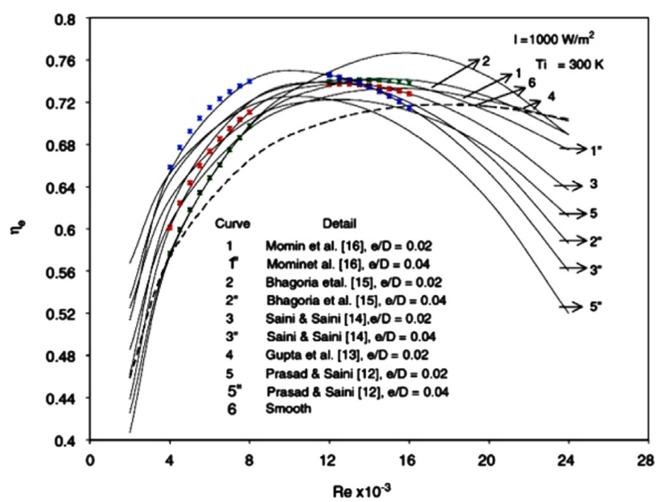


Fig. 17. Effective efficiency versus Reynolds number for roughened and smooth solar air heaters [43].

5.2. Thermal efficiency

The design of a solar air heater using artificial roughness can be based on the best thermal performance where the thermal performance of the collector is expressed in terms of useful energy gain by the collector per unit solar energy input and it can be determined as follows:

$$\eta_{th} = \frac{Q_u}{I\,A_P} \tag{18}$$

5.3. Enhancement of collector thermal performance

As studied earlier, the use of artificial roughness on the underside of absorber plate of the solar air heater leads to considerable enhancement in the heat transfer. These result in similar enhancement in the thermal efficiency of the solar collector [35]. Fig. 1 shows that there is substantial improvement in the thermal efficiency of solar air heater and that this enhancement is a strong function of roughness parameters.

Saini [35] investigated the thermal performance of solar air heater having artificially roughened absorber plate by fixing expanded metal matrix on it. The effect of roughness and operating parameters has been examined and a comparison of performance of roughened solar air heater with that of conventional solar air heater having smooth duct was made. Thermal performance plots for roughened as well as corresponding smooth air heaters have been prepared using experimental data under various operating parameters.

Fig. 2 shows the effect of relative roughness height, e/D on the thermal efficiency of solar air heaters. It indicates that with an increase in relative roughness height, the thermal efficiency increases. Fig. 3 shows the effect of relative longway length of the mess, L/e on thermal efficiency. These figure shows that the thermal efficiency increases with as increase in mass flow rate as also with decreasing values of temperature rise parameter.

Gupta et al. [15] experimentally investigated the thermal efficiency of solar air heater having artificially roughened absorber plate by fixing inclined rib on it. It has been shown that the thermal energy gain and pumping power increase with increase in flow rate. In the low flow rate range, thermal energy gain increases sharply with increase in flow rate while rate of pumping power consumption is low, resulting in higher value of effective efficiency. Beyond this range of flow rate, the rate of increase of pumping power is very high while the rate of useful energy gain becomes nearly constant resulting in decrease in the value of effective efficiency.

Karmare and Tikekar [36] studied the thermal efficiency of solar air heater having artificially roughened absorber plate by fixing metal grit ribs on it. Fig. 4 shows the thermal efficiency versus $(T_o - T_i)/I$ for different values of Reynolds number and relative roughness height of roughened solar air heaters. It is observed that for a particular value of Reynolds number thermal

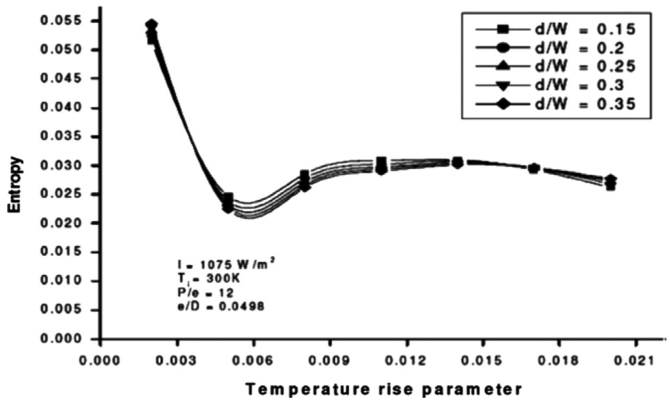


Fig. 18. Entropy versus temperature rise parameter for $P/e=12$ and $e/D=0.0498$ [52].

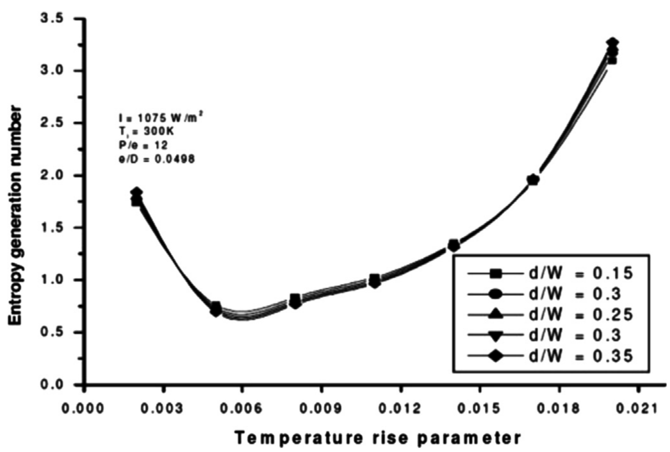


Fig. 19. Entropy generation number versus temperature rise parameter for $P/e=12$ and $e/D=0.0498$. $\Delta T/I$ [52].

efficiency increases with increase in $(T_o - T_i)/I$ at constant relative roughness height. It is also observed that thermal efficiency increases with relative roughness height.

Singh et al. [37] experimentally investigated the thermal efficiency of solar air heater having artificially roughened absorber by fixing discrete v-shaped ribs on it. The variation of thermal efficiency with Reynolds number and temperature rise parameter at different values of relative gap position for a fixed value of insolation and other roughness parameters is shown in Figs. 5 and 6, respectively. The thermal efficiency increases with the increase in relative gap position up to 0.65 and then decreases with further increase in relative gap position. The inter-rib local Nusselt number in the span-wise direction decreases continuously from the leading edges to the V-shaped apex of V-shaped down rib, the gap causes an increase in inter-rib local Nusselt number downstream of the gap. Therefore, depending upon the position of the gaps, the average heat transfer coefficient varies. If the gaps are created toward the V-shaped apex region, it will help in increasing the local heat transfer coefficient in the low heat transfer coefficient region; therefore, the average heat transfer coefficient and hence thermal efficiency is enhanced. This happens until the relative gap position of 0.65. If the gaps are placed too close to the V-shaped apex, it is anticipated that the two high heat transfer regions generated on the downstream side due to gaps in both legs of V-shaped rib may overlap, and therefore will not produce a similar effect of enhancement in the average heat transfer coefficient. Thus, placing the gaps closer to the V-shaped apex (d/W) 0.65 results in a lesser increase in average heat transfer coefficient and hence thermal efficiency. The enhancement in thermal efficiency increases as the relative gap position is increased from 0.20 to 0.35, and as the relative gap position is increased further there is a negligible change in enhancement

Figs. 7 and 8 show the variation of thermal efficiency with Reynolds number and temperature rise parameter, respectively, at different values of relative gap width. It has been concluded that the thermal efficiency is the highest at a relative gap width of 1.0 and decreases on both sides of this gap width. The inter-rib local heat transfer coefficient on the downstream side of the rib-gap is influenced by the flow velocity through the gap and area disturbed due to gap flow. As the gap width increases, the flow velocity reduces and the area disturbed increases. The two factors have opposing effects on local heat transfer coefficient. There exists an optimum relative gap width at which heat transfer coefficient and hence thermal efficiency is the highest. For the present study, the thermal efficiency is the highest corresponding to a relative gap width of 1.0. It has been concluded that the enhancement in thermal efficiency is much more as the relative gap width is increased from 0.50 to 1.0, and the enhancement decreases at a slower rate as the relative gap width is increased further.

6. Thermohydraulic performance of roughened solar air heaters

Studies have been conducted to develop methodologies for assessing the net heat gain in energy due to artificial roughness as augmentation of heat transfer vis-à-vis enhancement of pumping power requirement. Efforts have been made to optimize such a system for a required temperature rise if the heat transfer and the friction factor data are available. The existence of optimum condition for a given rough surface was proposed by Sheriff and Gumley [38]. It was shown that the characteristics of a roughened surface necessary to give the minimum pumping power, in the channel can be written as

$$\frac{f}{f_s} = \left(\frac{St}{St_s}\right)^3 \tag{19}$$

Performance of the roughened tubes in heat exchanger design relative to smooth tubes of equal diameter was studied by Webb and Eckert [39] with a view to obtain enhanced heat transfer capacity, to reduce the frictional power requirement and to permit a reduction of heat transfer surface area. They stated the design objectives for heat exchanger having tubes with inner smooth surfaces operating at fixed total rate and entering fluid temperature. The design objectives are summarized as

To obtain reduced heat transfer area for equal heat duty and pumping power

$(Q/Q_s = 1 \text{ and } P/P_s = 1)$

To obtain increased heat capacity for equal surface area and pumping power

$(A/A_s = 1 \text{ and } P/P_s = 1)$.

To reduce pumping power expenditure for equal heat transfer and surface area.

$(Q/Q_s = 1 \text{ and } A/A_s = 1)$.

The heat transfer enhancement Q/Q_s equals to the relative conductance $K/K_s = hA/h_sA_s$ for the rough and smooth tubes heat

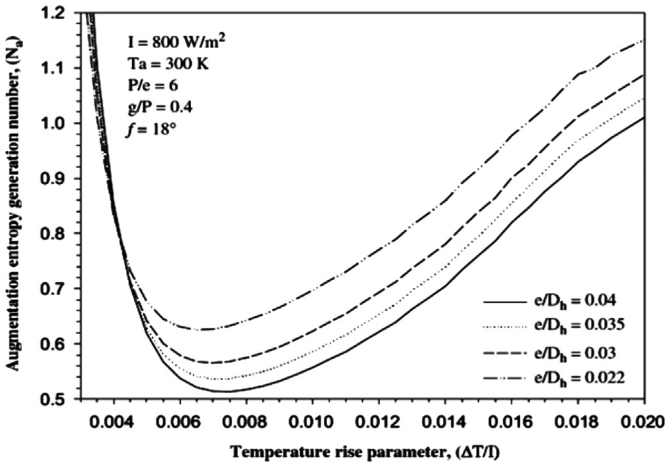


Fig. 20. The effect of relative roughness height on augmentation entropy generation number [53].

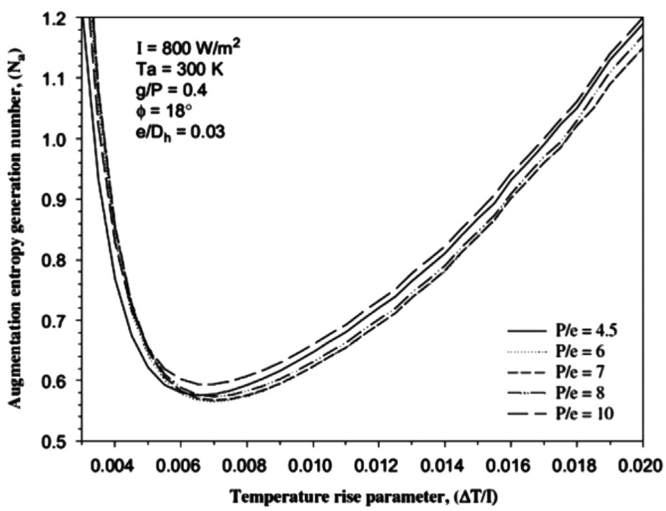


Fig. 21. The effect of relative roughness pitch on augmentation entropy generation number [53].

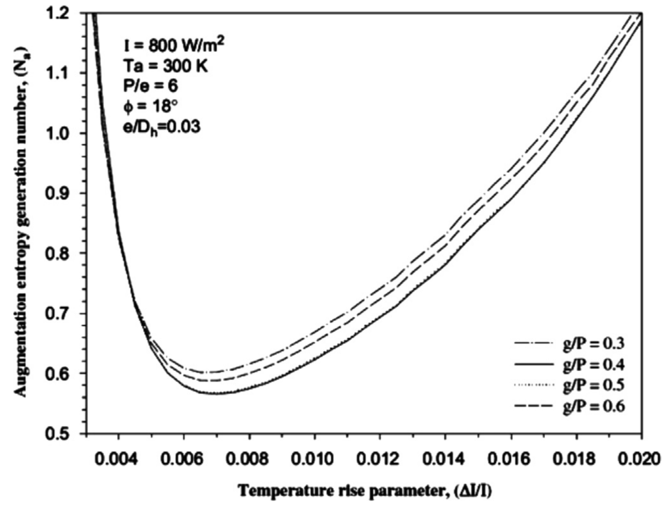


Fig. 22. The effect of relative groove position on augmentation entropy generation number [53].

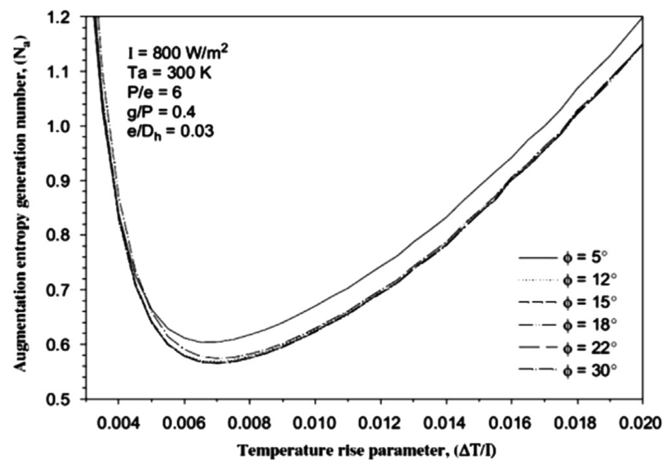


Fig. 23. The effect of chamfer angle on augmentation entropy generation number [53].

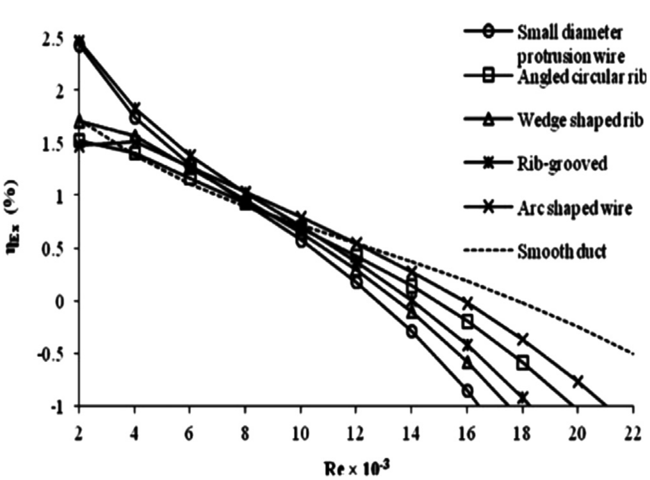


Fig. 24. Variation of exergy efficiency with Reynolds number for various roughness geometries (at $e/d=0.035$, $I=1000\ \mathrm{W/m^2}$ and $U_L=5\ \mathrm{W/m^2\text{-}K}$) [54].

exchangers. The relative conductance can be written as

$$K/K_s = \mathrm{St}/\mathrm{St}_s.A/A_s.\ G/G_s \tag{20}$$

The corresponding pumping power ratio is

$$P/P_s = f/f_s.A/A_s.\ (G/G_s)^3 \tag{21}$$

Webb et al. [39] specified that it may be necessary to operate the rough tube at a lower velocity than smooth tube for equal pumping power. If the heat exchanger mass flow rate and tube diameter are held constant, this may be accomplished by increasing the number of rough tubes (N) in parallel by ratio,

$$N/N_s = G/G_s.$$

Eliminating G/G_s from Eqs. (20) and (21)

$$\frac{K/K_s}{(P/P_s)(A/A_s)^{2/3}} = \frac{St/St_s}{(f/f_s)^{1/3}} \tag{22}$$

Eq. (22) provides an expression containing the parameters K/K_s, P/P_s, and A/A_s defined in terms of the ratios of friction factor and Stanton number f/f_s and $\mathrm{St}/\mathrm{St}_s$, respectively.

For each of three application cases stated above, two of these parameters are unity. Table 3 given the results of Eqs. (20) and (21) when applied to each of the three heat exchanger applications.

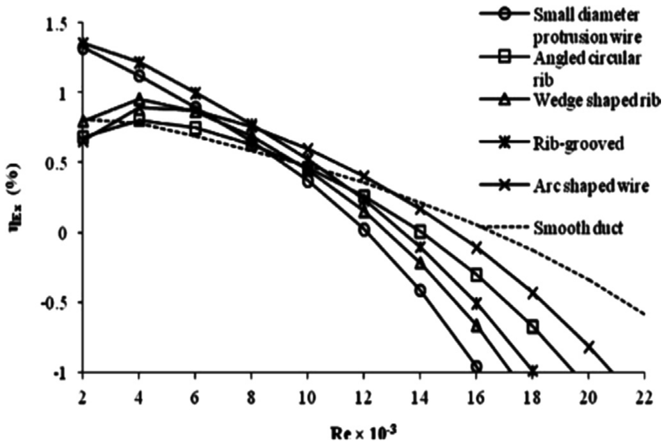


Fig. 25. Variation of exergy efficiency with Reynolds number for various roughness geometries (at $e/d=0.035$, $I=1000$ W/m^2 and $U_L=10$ W/m^2-K) [54].

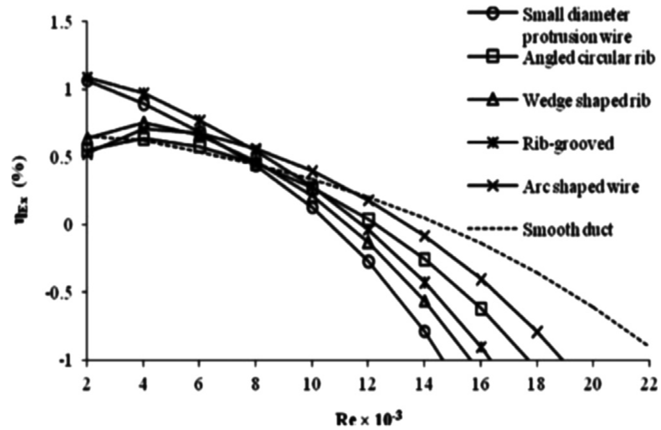


Fig. 27. Variation of exergy efficiency with Reynolds number for various roughness geometries (at $e/d=0.035$, $I=800$ W/m^2 and $U_L=10$ W/m^2-K) [54].

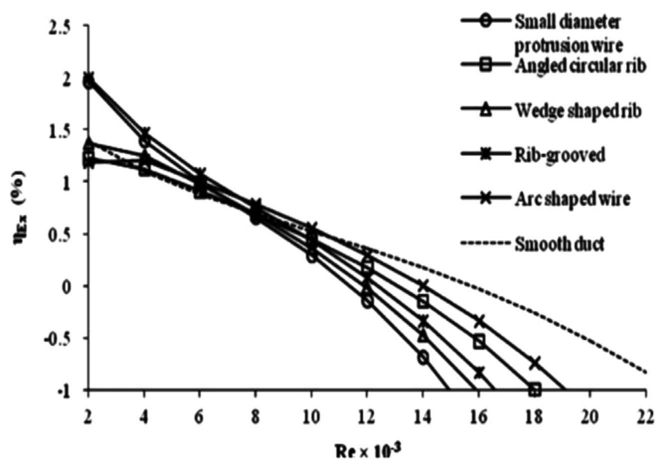


Fig. 26. Variation of exergy efficiency with Reynolds number for various roughness geometries (at $e/d=0.035$, $I=800$ W/m^2 and $U_L=5$ W/m^2-K) [54].

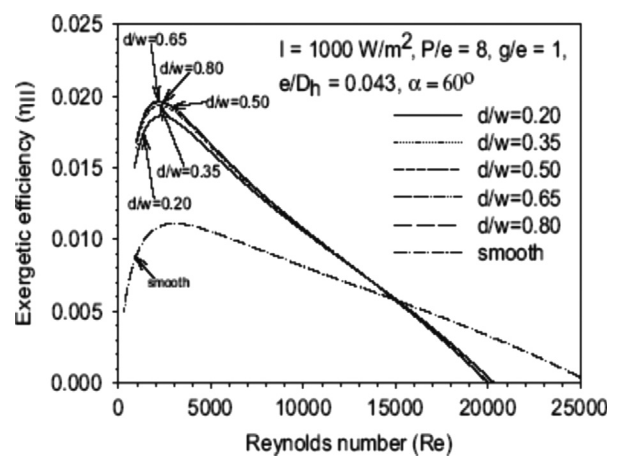


Fig. 28. Exergy efficiency as function of Reynolds number and relative gap position (d/W) [55].

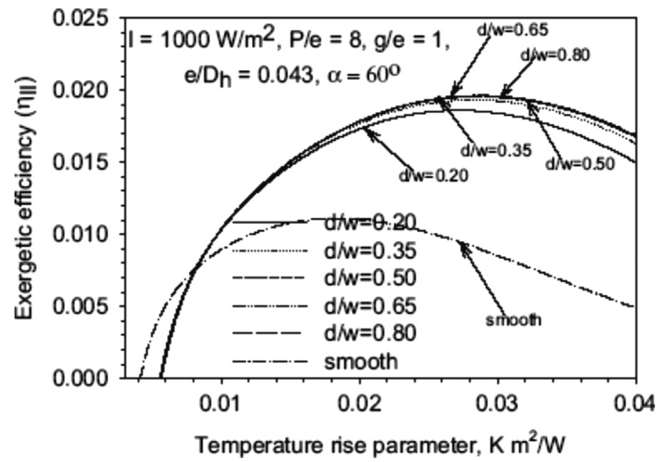


Fig. 29. Exergy efficiency as function of temperature rise parameter ($\Delta T/I$) and relative gap position (d/W) [55].

The last column of the Table 3 gives the relative mass velocity $G^{*}=G_s/G$ calculated from Eqs. (20) and (21) required to satisfy the constraints.

Lewis [40] proposed the criteria of evaluating the thermo-hydraulic performance of roughened surfaces by defining an optimization parameter called thermo hydraulic performance parameter η, which is expressed as follows:

$$\eta=(\mathrm{St}/\mathrm{St}_s)^3/(f/f_s) \tag{23}$$

The roughness that yields a value of this parameter greater than unity is useful and out of various possible sets, the one that yields the maximum value of this parameter should be used.

6.1. Effective efficiency

Cortes and Piacentini [41] defined the effective efficiency (η_{eff}) of solar air heater as the ratio of the net exergy gain to the energy available as insolation. The net energy gain is obtained by subtracting the pumping power from the energy gained by the air flowing through the collector. Thus, the effective efficiency represents the net gain per unit solar energy input. It is expressed as

$$\eta_{\mathrm{eff}}=\frac{Q_u-(P_m/C)}{IA_P} \tag{24}$$

where 'C' ($=\eta_f\eta_m\eta_{\mathrm{tr}}\eta_{\mathrm{th}}$) is the conversion factor accounting for net conversion efficiency from primary thermal energy to mechanical energy of pumping power.

η_f: efficiency of the fan,
η_m: efficiency of the electric motor,
η_{tr}: efficiency of electrical transmission from the power plant, and
η_{th}: efficiency of thermal conversion of the power plant.

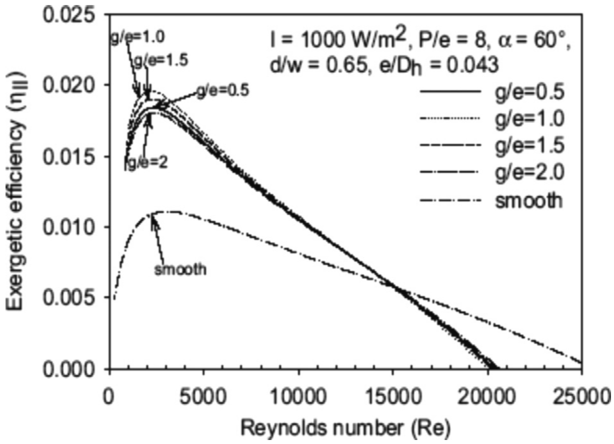


Fig. 30. Exergy efficiency as function of Reynolds number and relative gap width (g/e) [55].

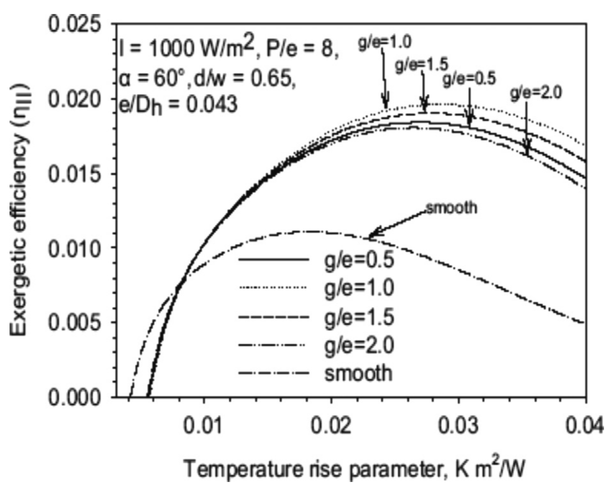


Fig. 31. Exergy efficiency as function of temperature rise parameter (ΔT/I) and relative gap width (g/e) [55].

The value of '*C*' as recommended by Cortes and Piacentini [41] is 0.18 (typical values of efficiency factors being: η_f=0.65, η_m=0.88, η_{tr}=0.925 and η_{th}=0.344).

Effective efficiency has been employed by several investigators [37,42,43,51–53] to account for the increase in mechanical energy, higher grade energy, expended in an effort to increase the thermal performance of the system as a result of use of artificial roughness.

Karwa et al. [42] experimentally investigated the thermal efficiency of solar air heater having artificially roughened absorber plate by fixing chamfered ribs on it. The enhancement in the Nusselt number due to the artificial roughness is found to be about 50–120% as shown in Fig. 9. Again the greatest enhancement in the Nusselt number has been observed for the air heater with the largest relative roughness height. The enhancement in the heat transfer rate has been found to result in a lower temperature of the roughened heated plate and in the increased outlet air temperature as compared to the smooth plate. Thus, the heat loss from the collector to the surroundings, which is proportional to the temperature excess of the heated plate over the ambient, is lower for the roughened collector. The artificial roughness on the heated plate that results in the desirable increase in the thermal efficiency also results in an undesirable increase in the pressure drop due to the increased friction. The friction factors for the roughened solar air heater ducts are about 1.8–2.3 times of that for the smooth duct solar air heater ducts for the relative roughness height of 0.0197 and about 3.1–3.9 times for the relative roughness height of 0.0441 as can be seen in Fig. 10.

Karmare and Tikekar [36] experimentally investigated the thermal as well as the effective efficiencies of solar air heater having artificially roughened absorber plate by fixing metal grit ribs on it. Fig. 11 shows the rate of useful energy gain and the power requirement of the fan as a function of Reynolds number. It is observed that the rate of increase of useful energy gain is relatively higher at low range of Reynolds number, whereas it is a bit lower at higher range of Reynolds number. But the rate of increase of power consumption is low for lower range of Reynolds number and increases relatively at high rate as Reynolds number, Re, increases. The power consumption does not exceed the rate of useful energy gain, i.e. the net energy gain rate is positive and it is also clear that at higher Reynolds number, the rate of useful energy collected becomes almost constant but the power consumption rises steeply. The thermal as well as the effective efficiencies of the collector as a function of Reynolds number, Re, are shown in Fig. 12 which shows that the thermal efficiency increases with Reynolds number, Re, whereas the effective efficiency attains a maximum value at a particular Reynolds number and thereafter decreases. This shows that an optimum operating condition does exist for the given roughness configuration at which the effective efficiency is maximum for a particular Reynolds number.

Singh et al. [37] experimentally investigated the effective efficiency of solar air heater having artificially roughened absorber by fixing discrete v-shaped ribs on it. Fig. 13 shows that that the optimum value of relative gap position for discrete V-shaped down rib-roughness varies with variation in Reynolds number. For Re=22,000 the effective efficiency is the highest at d/w=0.65, and for 22000 < Re > 27000 the effective efficiency is the highest at d/w=0.20. It has been concluded that the enhancement in effective efficiency is much more when d/w is increased from 0.20 to 0.35 as compared to when d/w is increased further, beyond d/w=0.65 the enhancement reduces. It is also observed in Figs. 13 and 14 that at higher Reynolds number or at lower, $\Delta T/I$ the effective efficiency of conventional flat plate solar air heater is more than the roughened solar air heaters. The friction factor ratio of V-shaped down rib-roughened ducts to that of smooth ducts increases with the increase in values of Reynolds number. Thus, as the Reynolds number increases, the pumping power for roughened duct increases at a much higher rate than that of smooth duct. Beyond a certain value of Reynolds number, the pumping power becomes much more for roughened solar air heater. Hence the roughened solar heaters have low effective efficiency at high Reynolds number. A similar trend is observed for temperature rise parameter, as shown in Fig. 14.

Fig. 15 shows the plot of effective efficiency as a function of Reynolds number for a different relative gap widths. It is seen that for Re=22000 the optimum relative gap width is 1.0, whereas for Reynolds number ranging from 22000 to 23000 and from 23000 to 28500 the optimum relative gap widths are 1.5 and 2.0, respectively. For Reynolds number of more than 28500, the smooth conventional solar air heater has the highest effective efficiency. It is observed from Fig. 16 that for $\Delta T/I$=0.0041 K m^2/W, the smooth conventional solar air heater has the highest effective efficiency. Beyond $\Delta T/I$ of 0.0041 K m^2/W, the discrete V-shaped down rib-roughened solar air heater has the higher efficiency. For $\Delta T/I$ range of 0.0041–0.0050 K m^2/W and 0.0050–0.0055 K m^2/W, the optimum relative gap widths are 2.0 and 1.5, respectively. For $\Delta T/I$=0.0055 K m^2/W the optimum relative gap width is 1.0. They showed that the considerable enhancement in effective efficiency as g/e is increased from 0.5 to 1.0, and as the g/e is increased further the enhancement decreases at a slower rate.

Mittal et al. [43] carried out a study in order to compare the effective efficiency of solar air heaters having different roughness geometries. It is seen from Fig. 17 that among all the roughness elements investigated, solar air heater having angled ribs of low roughness height (e/D) has been found to have better effective efficiency in higher range of Reynolds number (more than 12000). However, in lower range of Reynolds number (less than 12000) is the solar air heaters having expanded metal mesh as artificial roughness element have better efficiency. Further it is also observed that the effective efficiency of smooth solar air heater is better than the roughened solar air heaters in the range of very high Reynolds number. In order to determine the uncertainty in the results a sensitivity analysis has been carried out as shown in Fig. 17. In the lower range of Reynolds number the maximum value of uncertainty was found to be as 2.5% and for the expanded metal mesh geometry and for inclined ribs it has been observed as 0.8%. However, in the higher range of Reynolds numbers, the maximum uncertainty has been found to be as 0.5% and 0.4% for expanded metal mesh and angled ribs respectively.

6.2. Exergetic efficiency

Altfeld et al. [44] proposed a method for represents efficiency, based on the second law of thermodynamics to determine the optimum values of roughness geometry parameters. All energy flows are evaluated in terms of exergy. Exergetic efficiency, defined as a ratio of net exergy flow to exergy flow associated with solar irradiation on collector surface, which can be expressed as:

$$\eta_{\text{exg}} = \frac{E_n}{E_s} \tag{25}$$

Where E_n is net exergy flow rate and is expressed as

$$E_n = IA_P\eta_{\text{th}}\eta_c - P_m(1-\eta_c) \tag{26}$$

I is the global irradiation (W/m^2)
P_m is pumping power
η_c is the Carnot efficiency [$=(1-T_a/T_f)$]

E_s is the exergy associated with solar irradiation on collector surface and is given as

$$E_s = I\left(1-\frac{T_a}{T_{\text{sun}}}\right) \tag{27}$$

T_{sun} is the equivalent temperature of the Sun as a blackbody ($\approx$ 5762 K)

Exergy analysis, based on second law of thermodynamics, of renewable energy systems is gaining popularity amongst researchers and scientists as it deals with minimization of irreversibility and can indicate the possibilities of thermodynamic improvement of the process under consideration. Recently, the concept of exergy has been applied by many scientists [45–49,51] to optimize the performance of solar air heaters.

Suzuki [45] presented an exergy balance equation for a solar flat plate collector and an evacuated tubular collector. It was reported that both types of solar collectors have nearly equal capabilities in exergy gain despite large differences in technological efforts and expenses to produce them. Fujiwara [46] analyzed the performance of solar collectors from exergy point of view and stated that friction process, which is an energy conversion from mechanical energy to thermal energy, can be treated as exergy loss. Said and Zubair [47] analyzed the performance of two flat-plate solar collectors and a photovoltaic panel based on first as well as second law of thermodynamics. Second law efficiency values of 17% and 11% were obtained for photovoltaic and flat plate collectors respectively.

Naphon [48] presented a mathematical model for predicting the heat transfer characteristics, thermal performance and entropy generation of a double pass solar air heater having longitudinal fins. Effect of height and number of fins on the entropy generation was considered and it was found that with increase in height and number of fins, entropy generation decreases while thermal efficiency increases. Kurtbas and Durmus [49] experimentally evaluated the energy efficiency, friction factor and dimensionless exergy loss of a solar air heater having five solar sub-collectors of same length and width arranged in series in a common case for different values of Reynolds number. It was reported that temperature difference (T_o-T_i) of air, pressure loss and collector efficiency are the major parameters that affect the exergy loss. Ucar and Inalli [50] experimentally compared the performance and second law efficiency of flat plate solar collector having absorber plates of different shapes and orientations and reported that the least value of second law efficiency is obtained in case of a conventional collector. Gupta and Kaushik [51] undertook a comparative study to evaluate the performance of solar air heaters roughened with different roughness geometries on the basis of energy, effective and exergy efficiencies. It was found that artificial roughness on heated surface effectively increased the efficiencies in comparison to smooth surface. The thermal efficiency in general increased in the following sequence: smooth surface, circular ribs, v-shaped ribs, wedge shaped rib, expanded metal mesh, rib-grooved, and chamfered rib-groove. The effective efficiency based criteria also follows same trend of variation among various considered geometries, and trend was reversed at very high values of Reynolds number. The exergetic efficiency based criteria also follows the same pattern; however, the trend was reversed at relatively lower value of Reynolds number and for higher range of Reynolds number, the exergetic efficiency approaches zero or may be negative. It was found that for the higher range of Reynolds number, circular ribs and v-shaped ribs yield higher value of exergy efficiency while for low Reynolds number range, chamfered rib-groove yields higher value of exergetic efficiency.

Kumar et al. [52] experimentally investigated the effective efficiency of solar air heater having artificially roughened absorber by fixing discrete V-shaped ribs on it. Figs. 18 and 19 depict the effect of relative gap position on the entropy and entropy generation number. For the temperature rise parameter lower than 0.038 K/m^{2}W relative gap position of 0.15 has minimum value of entropy and entropy generation number. For the temperature rise parameter between 0.038 K/m^{2}W to 0.016 K/m^{2}W relative gap position of 0.35 has minimum entropy and entropy generation number. For the temperature rise parameter higher than 0.016 K/m^{2}W relative gap position of 0.15 has minimum value of entropy and entropy generation number.

Layek et al. [53] experimentally investigated the second law optimization of solar air heater having artificially roughened absorber by fixing chamfered rib-groove ribs on it. Fig. 20 shows the augmentation entropy generation number, Na as a function of temperature rise parameter and relative roughness height. It is evident that the ability of the chamfered rib-groove roughened absorber plate to reduce irreversibility depends on the thermo-fluid operating regime, and temperature rise parameter. The entropy generation rate decreases sharply with increase in temperature rise parameter reaches its minima for temperature rise parameter of about 0.007 K/m^{2}W and increases steadily with further increase in temperature rise parameter. The entropy generation decreases with the increase in relative roughness height. Fig. 21 depicts the effect of relative roughness pitch on the augmentation entropy generation number, Na. For the temperature rise parameter higher than 0.006 K/m^{2}W relative

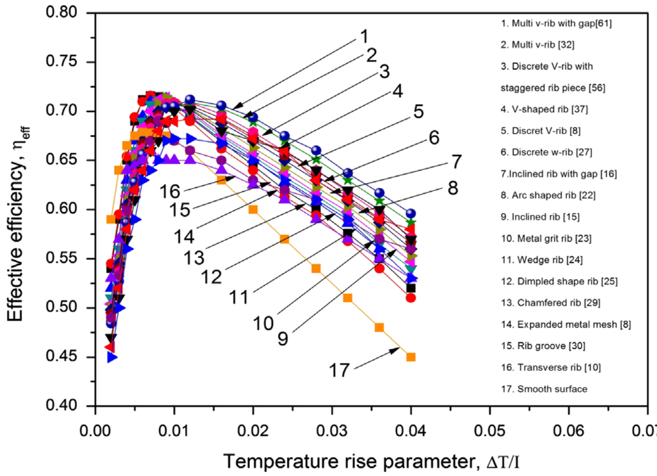


Fig. 32. Comparison various ribs with previous investigations.

roughness pitches of 6 have the best performance while the relative roughness pitch of 10 is the lowest. For the temperature rise parameter lower than 0.006 K/m^{2}W relative roughness pitches of 4.5 have the best performance.

Fig. 22 shows the effect of relative groove position on augmentation entropy generation number, Na. It can be seen that the relative groove position of 0.4 has the best performance for the temperature rise parameter of higher than 0.004 K/m^{2}W and 0.3 has the lowest. For the temperature rise parameter lower than 0.004 K/m^{2}W the trend is reversed. Fig. 23 shows the effect of chamfering of the rib top on augmentation entropy generation number, Na with variation in temperature rise parameter. It can be seen that due to change in chamfer angle from 51 to 181 has a remarkable effect.

Sharma and Varun [54] observed the variation in exergy efficiency (ηEx) with Reynolds number (Re) for different values of relative roughness height (e/D). It is seen from Figs. 24 to 27 that at low Reynolds number (less than 12000), the exergy efficiency increases with an increase the values of relative roughness height (e/D). However, it decreases rapidly at higher Reynolds number (beyond 12000). This is due to the fact that the rate of useful energy collected is less and the friction losses are more for higher values of relative roughness height. The effect of irradiance and overall heat loss coefficient are found to be is similar as discussed earlier. The exergy efficiency (ηEx) also follows similar trend, for different geometries, as shown in Figs. 3–6. For lower range of Reynolds number (up to 8000), rib-grooved ribs has better exergetic performance as compared to the other geometries. For moderate value of Reynolds number (up to 12000), solar air heater having arc shaped wire results in better exergetic efficiency. However, beyond 12000 Reynolds number values, smooth air heater is found to be better than that of a roughened solar air heater.

Singh et al.[55] experimentally compared the exergetic efficiency of flat plate solar collector having absorber plate of different shapes and orientations and reported that the optimum value of exergetic efficiency is obtained in case of a conventional collector. It can be seen from Fig. 28 that the highest η_{II} is obtained at d/w of 0.65 for Re < 13,000, and for Re > 15,300 the smooth conventional solar air heater results in the highest $\eta_{II.}$ For Reynolds number in the range of 13,000 to 15,300 different d/w are observed to result in the highest η_{II} depending on the Reynolds number. From Fig. 29 it is observed that for $\Delta T/I < 0.008$ Km^2/W the smooth conventional solar air heater results in the highest η_{II} and for $\Delta T/I > 0.0175$ Km^2/W the ribs having d/w of 0.65 results in highest η_{II}. For $\Delta T/I$ in the range of 0.008 to 0.0175 Km^2/W the highest η_{II} is observed for different d/w depending on value of $\Delta T/I$. The enhancement in exergetic efficiency is maximum at d/w of 0.65 except at low $\Delta T/I$. The enhancement is more when d/w is increased from 0.20 to 0.35 as compared to when d/w is increased further. The enhancement reduces at a slower rate as d/w is increased further.

Fig. 30 show that the highest η_{II} is obtained at g/e of 1.0 for Re < 12,500, and for Re > 15,200 the smooth conventional solar air heater results in the highest η_{II}. For the Reynolds number in range of 12,500–15,200, different g/e are observed to result in the highest η_{II} depending on the Reynolds number. From Fig. 31 it is observed that for $\Delta T/I < 0.008$ Km^2/W the smooth conventional solar air heater results in the highest η_{II}, and for $\Delta T/I > 0.0131$ Km^2/W the ribs having g/e of 1.0 results in the highest η_{II}. For $\Delta T/I$ in the range of 0.008 to 0.0131 Km^2/W the highest η_{II} is observed for different g/e depending on value of $\Delta T/I$. The exergetic efficiency is maximum at g/e of 1.0 except at low $\Delta T/I$. There is considerable enhancement in the exergetic efficiency as g/e is increased from0.5 to 1.0 and as the g/e is increased further the enhancement decreases at a slower rate.

Table 4
Fixed parameters.

S. no.	Description	Parameter	Value
1	Collector length, m	L	1.5
2	Collector width, m	W	1.0
3	Thermal conductivity of back insulated sheet, W/mK	k_i	0.037
4	Thickness of back insulated sheet, m	t_i	0.05
5	Density of air, kg/m^3	ρ	1.1541
6	Dynamic viscosity of air, kg/s-m	μ	1.865×10^{-5}
7	Thermal conductivity of air, W/mK	k	0.02624
8	Transmittance–absorptance product	$(\tau\alpha)$	0.8
9	Emissivity of absorber plate	ε_p	0.9
10	Emissivity of transparent glass sheet	ε_g	0.88
11	Ambient temperature, K	T_a	300
12	Wind velocity, m/s	V_w	1.0

7. Comparison effective efficiency of roughened solar air heaters duct

The solar air heater having artificially roughened absorber plate have higher heat transfer coefficient, through accompanied by an increase in friction factor. Correlations for Nusselt number and friction factor have been developed in terms of roughness and flow parameters by various investigators. A comparison of performance of roughened solar air heaters with that of conventional solar air heater s having different type roughness geometries namely here transverse continuous rib, inclined or angled rib, discrete V-shaped rib, arc shaped rib, metal grit rib, V-shaped rib, single V-shaped rib with staggered rib pieces, wedge shaped rib, w-shaped rib, continuous multi V-shaped rib, discrete multi V-shaped rib is being presented. These geometries /shapes have been chosen on the basis of the fact that they represent relatively more efficient artificial roughness systems.

7.1. System and variable parameters

The variable parameters comprise of roughness geometry i.e. relative roughness height (e/D), relative roughness pitch (P/e), relative width ratio (W/w), relative width gap (g/e) etc. and design parameters i.e. temperature rise parameter ($\Delta T/I$) and average

solar radiation intensity (I). The range of variable parameters representing roughness geometry has been selected on the basis of available correlation whereas the range of design parameters i.e. the temperature rise parameter and insolation has been decided on the basis of range of application of SAH and the insolation available at a place. As mentioned in Table 4 that the fixed parameters.

7.2. Procedure for prediction of effective efficiency

It may be noted that since the objective of this work is to present a methodology for optimal design of the solar air heater, the results need to be presented as function of two basic design parameters namely,

- Temperature rise parameter, $\Delta T/I$ (ratio of air temperature rise, ΔT, across the collector to the average intensity of solar insolation, I)
- Solar insolation (I)

The calculation starts with fixed value of these parameters ($\Delta T/I$ and I) and proceeds with the calculation of the other parameters for a given collector. Step by step procedure of calculation is given below

Step 1. A set of values of the roughness parameters namely relative roughness height (e/D), relative roughness width (W_D/W_R), wedge angle (Φ), relative staggered rib position (P'/P), relative discrete distance (G_d/L_v), relative discrete width (g/e), relative staggered rib size (r/e), relative discrete position (S'/S), angle of attack (α), relative roughness pitch (P/e) and angle of attack (α) is selected for which the calculation is to be performed.

Step 2. A set of values of design parameters namely temperature rise parameter, ($\Delta T/I$) solar insolation, I is selected.

Step 3. Area of plate is calculated as,

$$A_p = W \times L \tag{28}$$

Step 4. Hydraulic diameter of duct is calculated as;

$$D = \frac{2(W \times H)}{W + H} \tag{29}$$

Step 5. Fixed system parameters such as;
Thermal conductivity of insulation, k_i
Thickness of insulation, t_i
Transmittance–absorptance product, $(\tau\alpha)$
Emissivity of the absorber plate, ε_p
Emissivity of the glass covers, ε_g
Fixed operating parameters such as;
Atmospheric air velocity (V_w) and atmospheric temperature (T_a) are selected.

Step 6. The temperature rise ΔT of air and outlet temperature T_o is calculated as,

$$\Delta T = \frac{\Delta T}{I} \times I \tag{30}$$

$$T_o = \Delta T + T_i \tag{31}$$

Step 7. Approximate initial mean plate temperature is assumed as;

$$T_P = \frac{T_o + T_i}{2} + 10\ ^{\circ}\mathrm{C} \tag{32}$$

Step 8. Using the value of the plate temperature T_p, value of top loss coefficient, U_t is computed by using equation given as,

$$U_t^{-1} = \left[\frac{\sigma(T_P^2 + T_g^2)(T_P + T_g)}{((1/\varepsilon_P) + (1/\varepsilon_g) - 1)} + \left(\frac{k_a Nu}{L_g}\right)\right]^{-1} + [\sigma\varepsilon_g(T_P^2 + T_g^2)(T_P + T_g) + h_W]^{-1} + \frac{t_g}{k_g} \tag{33}$$

where

$$T_g = \left(\frac{F_1 T_P + cT_a}{1 + F_1}\right)$$

where,

$$F_1 = \frac{[12 \times 10^{-8}(T_a + 0.2T_P)^3 + h_W]^{-1} + 0.3t_g}{\left[6 \times 10^{-8}(\varepsilon_P + 0.028)(T_P + 0.5T_a)^3 + 0.6L_g^{-0.2}\{(T_P - T_a)\cos\beta\}^{0.25}\right]^{-1}}$$

and

$$c = \left(\frac{(T_s/T_a) + (h_W/3.5)}{(1 + (h_W/3.5))}\right)$$

$$T_s = 0.0522(T_a)^{1.5}$$

$$\mathrm{Nu} = 1 + 1.44[1 - 1708/\mathrm{Ra}\cos\beta]^{+} \times \{1 - 1708(\sin 1.8\beta)^{1.6}/\mathrm{Ra}\cos\beta\} + [(\mathrm{Ra}\cos\beta/5830)^{0.33} - 1]$$

where, $\mathrm{Ra} = G_r \times P_r$

$$G_r = \frac{g\beta'(T_P - T_g)L_g^3}{\nu^2}$$

$$\beta' = \frac{1}{[(T_o + T_i)/2]}$$

$$P_r = \frac{\mu C_P}{k_a}$$

Back loss coefficient U_b is expressed as;

$$U_b = k_i/t_i$$

The edge loss coefficient, based on the collector area A_P is given as;

$$U_e = \frac{(L + W)t_e k_i}{LWt_i}$$

finally,

$$U_L = U_t + U_b + U_e \tag{34}$$

Step 9. Useful energy gain is calculated as;

$$Q_{u1} = [I(\tau\alpha) - U_L(T_P - T_a)]A_P \tag{35}$$

Step 10. Mass flow rate is determined from the expression given as;

$$m = \frac{Q_{u1}}{C_P \Delta T} \tag{36}$$

Step 11. Reynolds number of flow of air in the duct is computed as;

$$\mathrm{Re} = \frac{\mathrm{GD}}{\mu} \tag{37}$$

where, G is the mass velocity of air through the collector

$$G = \frac{m}{WH} \tag{38}$$

Step 12. The Nu is calculated using the correlation given for a particular type of roughness geometry. The correlations for Nu and f are given in Table 3 for the roughness shapes and geometries that have been chosen for the present investigation.

Step 13. The convective heat transfer coefficient is calculated as follows,

$$h = \frac{\mathrm{Nu}\,k}{D} \tag{39}$$

Step 14. The plate efficiency factor is then determined as,

$$F' = \frac{h}{h + U_L} \tag{40}$$

Step 15. The heat removal factor is calculated as,

$$F_o = \frac{mC_P}{A_P U_L}\left[\exp\left\{\frac{F' U_L A_P}{mC_P}\right\} - 1\right] \tag{41}$$

Step 16. The useful heat gain, Q_{u_2} is computed as,

$$Q_{u_2} = F_o A_P [I(\tau\alpha) - U_L(T_o - T_i)] \tag{42}$$

Step 17. At this stage, the difference between the two values of useful heat gain Q_{u_1} and Q_{u_2} is checked. Ideally the two values should be same. However, if the difference in two values is more than 0.1% of Q_{u_1}, then the plate temperature is modified as,

$$T_P = T_a + \left[\frac{I(\tau\alpha) - (Q_{u_2}/A_P)}{U_L}\right] \tag{43}$$

Step 18. Using the new plate temperature, the calculations from Step 6–17 are performed again till the difference between the two values of useful heat gain, Q_{u_1} and Q_{u_2} is reduced to a value below 0.1% of Q_{u1}.

Step 19. Friction factor, f is calculated using the correlations given for a particular type of roughness geometry. The correlations used for f are given in Table 3 which is to be used for analysis.

Step 20. Using the value of f, the pressure drop $(\Delta P)_d$, across the duct is calculated as follow:

$$(\Delta P)_d = \frac{4fL\rho V^2}{2D} \tag{44}$$

Step 21. Using the value of (ΔP)d, the mechanical power (P_m) is calculated as,

$$P_m = \frac{m(\Delta P)_d}{\rho} \tag{45}$$

Step 22. Thermal efficiency is calculated as;

$$\eta_{\mathrm{th}} = F_o\left[(\tau\alpha) - \frac{U_L(T_o - T_i)}{I}\right] \tag{46}$$

Step 23. The effective efficiency, η_{eff}, is calculated as;

$$\eta_{\mathrm{eff}} = \frac{Q_u - (P_m/C)}{I.A_p} \tag{47}$$

The effects of $\Delta T/I$ and geometric parameters of roughness on effective efficiency in an solar air heater duct is presented and discussed in this section. The results of the roughened solar air heater duct are also compared with solar air heater ducts with smooth surface for similar $\Delta T/I$ values and numerical conditions. Fig. 32 shows the effective efficiency, respectively, as functions of $\Delta T/I$ for various roughness geometries.

Kumar et al. [61] showed that discrete multi V-ribs on the underside of the absorber plate of an solar air heater duct amplifies thermal as well as hydraulic efficiencies. They concluded that the higher heat transfer rate is attributed to the interaction of secondary flow released through the discrete in multiple V-rib roughness with the main flow. The higher thermal performance is attributed to the interaction of the secondary flow released through the discrete with the main flow. This increases effective efficiency through the discrete width area behind the discrete. Discrete multi V-ribs performed better than non-discrete multiple V-ribs. As shown in Fig. 36, the multi V-with gap rib geometry results in the best effective efficienct among all the roughness shapes investigated. Tables 2 and 3 gives the range of optimum roughness rib parameters and thermohydraulic performance parameters compared with previous studies.

8. Conclusions

(i) The literature review shows that the use of artificial roughness in different forms and shapes is an effective and economic way of improving the performance of solar air heaters.

(ii) Numbers of experimental investigations involving roughness elements of different shapes, sizes and orientations with respect to flow direction have been carried out in order to obtain an optimum arrangement of roughness element geometry.

(iii) Correlations for heat transfer and friction factor have been developed which are applicable to wide range of rib configurations and operating parameters.

(iv) It is found that in case of transverse ribs, two fluid vortices immediately upstream and downstream of rib are stagnant on account of which fluid temperature as well as wall temperature increase resulting in low heat transfer.

(v) Angling of transverse rib further enhances the heat transfer on account movement of vortices along the rib and formation of a secondary flow cell near the leading end, which results in local wall turbulence. V-shaping of a long angled rib helps formation of secondary flow cells as compared single transverse ribs.

(vi) Creating gap in V-shaped rib is found to enhance the heat transfer rate by breaking the secondary flow and producing higher level of turbulence in the fluid downstream of the rib. Multi v-shaped rib further enhances the heat transfer rate because increase the number of secondary flow cells several times.

(vii) Methodology of artificial roughness and experimental studied carried out by various investigators have been discussed and reported in detail. Concept of thermal efficiency, thermohydraluic performance (effective efficiency) and exergy efficiency has been discussed. It is observed that artificial roughness is a good technique to improve the thermohydraulic performance of solar air heaters.

(viii) The enhancements in the Nusselt number, friction factor and thermal efficiency are found to be strong functions of the relative roughness height. The greatest enhancement is observed for the air heater with the highest relative roughness height. The effective efficiency of a roughened solar air heater increases as the insloation increases for Reynolds numbers higher than 10,000–12,000. However at lower

Reynolds number the thermohydraulic efficiency decreases with increasing insolation.

(ix) Most of the technique used for optimized the roughness geometries used in solar air heater for optimum values of roughness geometry parameters as a function of operating conditions of solar air heater have been determined on the basis of thermal efficiency, effective efficiency and exergetic efficiency criteria.

References

[1] Duffie JA, Beckman WA. Solar Engineering Thermal Processes. New York: John Wiley; 1991.
[2] Sukhatme SP. Solar Energy Engineering. New Jersey: Printice Hall Inc.; 1986.
[3] Veziroghu TN. Solar Energy International Progress. London: Pergamon Press; 1980; 167–73.
[4] Hsieh JS. Solar Energy Engineering. New Jersey: Printice Hall Inc.; 1986.
[5] Helmbold, W.. In: Proceeding international workshop on energy conservation in buildings. CBRI: Roorkee; 1984 p. 30.
[6] Close DJ. A design approach for solar processes. Sol Energy 1967;11:112–22.
[7] Mills DR. The plate of extreme asymmetrical non-focussing concentrators in solar energy utilization. Sol Energy 1978;21:431–4.
[8] Hans VS, Saini RP, Saini JS. Performance of artificially roughened solar air heaters-A review. Renew Sustain Energy Rev 2009;13:1854–69.
[9] Prasad K, Mullick SC. Heat transfer characteristics of a solar air heater used for drying purpose. Appl Energy 1983;13:83–93.
[10] Prasad BN, Saini JS. Effect of artificial roughness on heat transfer and friction factor in a solar air heater. Sol Energy 1988;41:555–60.
[11] Prasad BN, Saini JS. Optimal thermohydraulic performance of artificially roughened solar air heaters. Sol Energy 1991;47(1991):91–6.
[12] Verma SK, Prasad BN. Investigation for the optimal thermohydrailuc performance of artificially roughened solar air heaters. Renew Energy 2000;20:19–36.
[13] Karwa RK. Experimental studies of augmented heat transfer and friction in asymmetrically heated rectangular ducts with ribs on heated wall in transverse, inclined, v-continuous and v-discrete pattern. Int Commun Heat Mass Transf 2003;30:241–50.
[14] Sahu MM, Bhagoria JL. Augmentation of heat transfer coefficient by using 90 broken transverse ribs on absorber plate of solar air heater. Renew Energy 2005;30:2075 (2063).
[15] Gupta D, Solanki SC, Saini JS. Thermohydraulic performance of solar air heaters with roughened absorber plates. Sol Energy 1997;61:33–42.
[16] Aharwal KR, Gandhi BK, Saini JS. Experimental investigation on heat-transfer enhancement due to a gap in an inclined continuous rib arrangement in a rectangular duct of solar air heater. Renew Energy 2008;33:585–96.
[17] Momin AME, Saini JS, Solanki SC. Heat transfer and friction in solar air heater duct with v-shaped rib roughness on absorber plate. Int J Heat Mass Transf 2002;45:3383–96.
[18] Varun Saini RP, Singal SK. A review on roughness geometry used in solar air heaters. Sol Energy 2007;81:1340–50.
[19] Karwa R, Bairwa RD, Jain BP, Karwa N. Experimental study of the effects of rib angle and discretization on heat transfer and friction in an asymmetrically heated rectangular duct. J Enhanc Heat Transf 2005;12(2005):343–55.
[20] Karwa R, Solanki SC, Saini JS. Heat transfer coefficient and friction factor correlations for the transitional flow regime in rib roughened rectangular ducts. Int J Heat Mass Transf 1999;42:1597–615.
[21] Saini RP, Saini JS. Heat transfer and friction factor correlations for artificially roughened ducts with expanded metal mesh as roughened element. Int J Heat Mass Transf 1997;40(1997):973–86.
[22] Saini SK, Saini RP. Development of correlations for Nusselt number and friction factor for solar air heater with roughened duct having arc-shaped wire as artificial roughness. Sol Energy 2008;82(2008):1118–30.
[23] Karmare SV, Tikekar AN. Heat transfer and friction factor correlation for artificially roughened duct with metal grit ribs. Int J Heat Mass Transf 2007;50:4342–51.
[24] Bhagoria JL, Saini JS, Solanki SC. Heat transfer coefficient and friction factor correlations for rectangular solar air heater duct having transverse wedge shaped rib roughness on the absorber plate. Renew Energy 2002;25:341–69.
[25] Saini RP, Verma J. Heat transfer and friction factor correlations for a duct having dimple-shaped artificial roughness for solar air heaters. Energy 2008;133:1277–87.
[26] Lanjewar A, Bhagoria JL, Sarviya RM. Experimental study of augmented heat transfer and friction in solar air heater with different orientations of w-rib roughness. Exp Thermal Fluid Sci 2011;35:986–95.
[27] Kumar, A, Bhagoria, JL, Sarviya, RM.. In: Proceedings of the international 19th national and 8th ISHMT-ASME heat and mass transfer. 2008.
[28] Varun Saini, Singal RP, S. K.. Investigation of thermal performance of solar air heater having roughness elements as a combination of inclined and transverse ribs on the absorber plate. Renew Energy 2008;33:1398–405.
[29] Layek A, Saini JS, Solanki SC. Heat transfer coefficient and friction characteristics of rectangular solar air heater duct using rib-grooved artificial roughness. Int J Heat Mass Transf 2007;50:4845–54.
[30] Jaurker AR, Saini JS, Gandhi BK. Heat transfer and friction characteristics of rectangular solar air heater duct using rib-grooved artificial roughness. Sol Energy 2006;80:895–907.
[31] Bopche SB, Tandale MS. Experimental investigations on heat transfer and friction characteristics of a tabulator roughened solar air heater. Int J Heat Mass Transf 2009;67(2009):39.
[32] Hans VS, Saini RP, Saini JS. Heat transfer and friction factor correlations for a solar air heater duct roughened artificially with multiple v-ribs. Sol Energy 2010;84(2010):898–911.
[33] ASHRAE Standard 93–77. Method of testing to determine the thermal performance of solar air heater. New York; 1977. p. 1–34.
[34] Biondi P, Cicala L, Farina G. Performance analysis of solar air heaters of conventional design. Sol Energy 1988;41:101–7.
[35] Saini RP. Study of enhancement of energy collection rates of solar collectors using artificial roughness in the air duct. Roorkee: University of Roorkee; 1996 (Ph.D. Thesis).
[36] Karmare SV, Tikekar AN. Experimental investigation of optimum thermohydraulic performance of solar air heaters with metal rib grits roughness. Sol Energy 2009;83:6–13.
[37] Singh S, Chander S, Saini JS. Thermal and effective efficiency based analysis of discrete V-down rib roughened solar air heaters. J Renew Sustain Energy 2011;3:023107.
[38] Sheriff N, Gumley P. Heat transfer and friction properties of surfaces with discrete roughnesses. Int J Heat and Mass Transf 1966;9:1297–320.
[39] Webb RL, Eckert RG, Goldstein RJ. Heat transfer and friction in tubes with repeated-rib roughness. Int J Heat Mass Transf 1971;26:601–17.
[40] Lewis MJ. Optimizing the thermohydraulic performance of rough surfaces. Int J Heat and Mass Transf 1975;18:1243–8.
[41] Cortes A, Piacentini R. Improvement of efficiency of a bare solar collector by means of turbulence promoters. Appl Energy 1990;36:253–61.
[42] Karwa R, Solanki SC, Saini JS. Thermo-hydraulic performance of solar air heaters having integral chamfered rib roughness on absorber plates. Energy 2001;26:161–76.
[43] Mittal MK, Varun, Saini RP, Singal SK. Effective efficiency of solar air heaters having different types of roughness elements on the absorber plate. Energy 2007;32:739–45.
[44] Altfeld K, Leiner W, Fiebg M. Second Law optimization of flat plate solar air heaters. Sol Energy 1988;41(1988):309–17.
[45] Suzuki A. A fundamental equation for exergy balance on solar collectors. J. Solar Energy Eng. 1988;110:102–6.
[46] Fujiwara M. Exergy analysis for the performance of solar collectors. J. Solar Energy Eng. 1983;105:163–7.
[47] Said SAM, Zubair SM. On second- law efficiency of solar collectors. J. Solar Eng. 1993;115:2–4.
[48] Naphon P. On the performance and entropy generation of the double pass solar air heater with longitudinal fins. Renew Energy 2005;30:1345–57.
[49] Kurtbas I, Durmus A. Efficiency and exergy analysis of a new solar air heater. Renew Energy 2004;29:1489–501.
[50] Ucar A, Inalli M. Thermal and exergy analysis of solar air collectors with passive augmentation techniques. Int J Heat Mass Transf 2006;33:1281–90.
[51] Gupta MK, Kaushik SC. Performance evaluation of solar air heater having expanded metal mesh as artificial roughness on absorber plate. Int J Thermal Sci 2009;48:1007–16.
[52] Kumar TS, Mittal V, Thakur TS. Second law analysis of a solar air heater having 60° inclined discrete rib roughness on absorber plate. Afr J Environ Sci Technol 2010;13:913.
[53] Layek A, Saini JS, Solanki SK. Second law optimization of a solar air heater having chamfered rib-groove roughness on absorber plate. Renew Energy 2007;32:1967–80.
[54] Sharma M, Varun. Performance estimation of artificially roughened solar air heater duct provided with continuous ribs. Int J Energy Environ 2010;5:897–910.
[55] Singh S, Chander S, Saini JS. Heat transfer and friction factor correlations of solar air heater ducts artificially roughened with discrete V-down ribs. Energy 2011;36:5053–64.
[56] Patil AK, Saini JS, Kumar K. Nusselt number and friction factor correlations for solar air heater duct with broken V-down ribs combined with staggered rib roughness. J Renew Sustain Energy 2012;4:033122.
[57] Patil AK, Saini JS, Kumar K. Heat transfer and friction characteristics of solar air heater duct roughened by broken V-shape ribs combined with staggered rib pieces. J Renew Sustain Energy 2011;4(1):013115–7.
[58] Patil AK, Saini JS and Kumar K. Effect of gap position in broken V-rib roughness combined with staggered rib on thermohydraulic performance of solar air heater. Green 1(4):329–8.
[59] Sethi M Varun, Thakur NS. Correlations for solar air heater duct with dimpled shape roughness elements on the absorber plate. Solar Energy 2012;86:2852–61.
[60] Kumar A, Saini RP, Saini JS. Development of correlations for Nu and f for SAH with roughened duct having multi v-shaped with gap rib as artificial roughness. Renew Energy 2013;58:151–63.
[61] Kumar A, Saini RP, Saini JS. Experimental investigation on heat transfer and fluid flow characteristics of air flow in a rectangular duct with multi v-shaped rib with gap roughness on the heated plate. Solar Energy 2012;86:1733–49.